

HIGH SPEED TRANSCUTANEOUS OPTICAL  
TELEMETRY LINK

By

DOUGLAS MICHAEL ACKERMANN, JR.

Submitted in partial fulfillment of the requirements

For the degree of Master of Science

Thesis Advisor: Dr. P. Hunter Peckham

Department of Biomedical Engineering  
CASE WESTERN RESERVE UNIVERSITY

May 2007

SIGNATURE PAGE

Replace this page with the committee signoff page.

SIGNATURE PAGE .....	ii
LIST OF TABLES .....	4
LIST OF FIGURES .....	5
ACKNOWLEDGEMENTS .....	6
ABSTRACT .....	7
CHAPTER I: EXTENDED INTRODUCTION .....	9
A. Motivation for a High Speed Transcutaneous Telemetry Link .....	9
B. Link Design Specifications .....	11
1) Functional Specifications .....	11
2) Technical Specifications .....	12
C. Fundamentals of Data Transfer .....	16
D. Choosing a Method for Data Transmission .....	17
E. Fundamentals of Optical Communication .....	21
1) Optical Transmitters .....	22
2) Optical Detectors .....	23
3) Optics and Filtering .....	24
4) Transmission Medium and Transmitter-Receiver Alignment .....	25
5) Noise in Optical Communication Systems .....	26
6) Multipath Distortion: Intersymbol Interference (ISI) .....	28
F. Optical Properties of Skin .....	28
1) The Layers of Human Skin .....	29
2) The UV, Visible and IR spectrum .....	29
3) Chromophores .....	31
4) Light Propagation in Human Skin .....	31
5) Optical Clearing .....	36
G. Optical Safety Hazards .....	36
1) Irradiative Heating .....	37
2) Conductive Heating .....	38
H. Conclusions .....	40
CHAPTER II: DESIGNING THE OPTICAL INTERFACE OF A TRANSCUTANEOUS	
OPTICAL TELEMETRY LINK .....	45
A. Abstract .....	45
B. Introduction .....	46
C. Experimental Methods .....	48
1) Tissue Preparation .....	48
2) Measurement Technique .....	48

3) Data Analysis.....	49
D. Optical Interface Theory.....	50
E. Results.....	55
1) Transmitted Optical Power Distribution.....	55
2) Optical Interface.....	60
F. Discussion.....	64
1) Transmitted Optical Power Distribution.....	64
2) Optical Interface.....	66
G. Conclusions.....	67
H. Acknowledgements.....	67
I. Chapter II Citations.....	68
<b>CHAPTER III: A HIGH SPEED TRANSCUTANEOUS OPTICAL TELEMETRY LINK</b>	

74

A. Abstract.....	74
B. Introduction.....	74
C. Architecture.....	79
1) Transmitter.....	79
2) Receiver.....	79
3) Optical Interface.....	80
D. Methods.....	80
1) Simulation of Transmission Errors.....	80
2) Measurement of Filter Efficacy.....	84
3) Measurement of Bit Error Rate.....	84
4) Lens Viewing Area Optimization.....	85
E. Results.....	87
1) Simulation of Transmission Errors.....	87
2) Filter Efficacy.....	89
3) Optical Interface.....	91
4) Bit Error Rate.....	91
5) Lens Viewing Area Optimization.....	94
F. Discussion.....	97
G. Conclusions.....	100
H. Acknowledgements.....	100
I. Chapter III Citations.....	101
<b>CHAPTER IV: Future Directions for implementing a transcutaneous optical telemetry</b>	

link 105

A. Abstract.....	105
B. Implementation with the Networked Neural Prosthesis System.....	105
C. Architecture of a Clinical Transcutaneous Optical Telemetry Link.....	109
1) Transmitter Design.....	109
2) Receiver Design.....	110
3) Implant Location.....	110

4) Device Packaging.....	111
5) Device Powering.....	112
6) Receiver-Transmitter Alignment Stability.....	112
7) Data Modulation .....	112
8) Hardware for the Data Link Layer.....	113
D. Conclusions.....	114
APPENDIX I: DATA MODULATION AND ERROR CONTROL .....	116
A. Data Modulation .....	116
B. Error Control Coding.....	119
CITATIONS FOR CHAPTERS I AND IV .....	121

## LIST OF TABLES

Table 1-1.....	25
Table 2-1.....	48

## LIST OF FIGURES

Figure 1-1.....	3
Figure 1-2.....	23
Figure 1-3.....	26
Figure 1-4.....	28
Figure 1-5.....	32
Figure 2-1.....	44
Figure 2-2.....	47
Figure 2-3.....	49
Figure 2-4.....	51
Figure 2-5.....	52
Figure 2-6.....	53
Figure 3-1.....	71
Figure 3-2.....	73
Figure 3-3.....	76
Figure 3-4.....	78
Figure 3-5.....	80
Figure 3-6.....	82
Figure 3-7.....	83
Figure 3-8.....	85
Figure 3-9.....	86
Figure 4-1.....	104
Figure 4-2.....	105

## ACKNOWLEDGEMENTS

This work would not have been possible without the assistance and support of many. I would like to first thank my advisor, Dr. Hunter Peckham, for his support and unique style of advising. It's been fun, and I'm looking forward to more. I would like to thank Dr. Kevin Kilgore, who acted as much more than a committee member, and was very generous with his time. I would also like to thank Dr. Darrin Young for his help and time serving on my committee.

I would like to thank Brian Smith, to whom I owe a debt of gratitude for his incredible generosity with his time, skill and knowledge.

I would like to thank Fred Montague, Jeff Weisgarber, Jim Buckett, Jim Uhlir, Tim Crish and Tom Stage for their technical advice and assistance. I would also like to thank Xiaofeng Wang for his statistical assistance, and Dawn Taylor's BCI lab for providing me with cortical recording data.

I want to thank all of my friends in the NEC who helped me with technical issues, and who helped me to forget technical issues over the last 2 ½ years.

I also want to take this opportunity to thank my loving parents and sister, who have always been there, and provided incredible support.

My deepest gratitude goes to Liz, for all of her love, encouragement, willingness to tolerate strange hours, constant smiles, inspiration and incredible friendship. Thank you.

# High Speed Transcutaneous Optical Telemetry Link

## ABSTRACT

by

DOUGLAS MICHAEL ACKERMANN, JR.

A transcutaneous optical telemetry link was constructed that is capable of transmitting the 40 Mbps of data generated by a 100 channel microelectrode recording array. To construct this link, an analysis of the transmitter-skin-receiver interface was performed. This analysis required empirically measured distributions of transmitted power from porcine skin samples, and demonstrated significant changes in power distribution shape and total power transfer with different skin thickness. This analysis demonstrated the tradeoffs between the fundamental optical interface design parameters, and allowed for the directed design of the actual hardware link. The optical link design was shown to be capable of transmitting data at a rate of 40 Mbps through 3 mm thick porcine skin, consuming an average emitter power of only 4.3 mW.

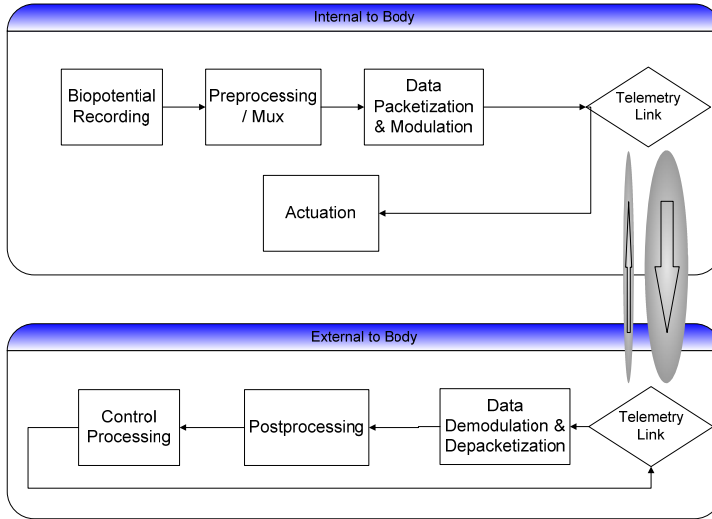
## **CHAPTER I: EXTENDED INTRODUCTION**

## CHAPTER I: EXTENDED INTRODUCTION

### *A. Motivation for a High Speed Transcutaneous Telemetry Link*

In some neural prosthetic applications there is a need for high bandwidth communication between an implanted device and an external device. For example, recent advances have demonstrated the feasibility of real-time cortical interfacing systems [1]-[4]. These systems utilize multiple parallel recordings from microelectrodes or microwires placed in the cortex, and are being developed as a prosthetic control source for the mobility impaired. Potential applications include the control of functional electrical stimulation, FES, systems, which can restore function to individuals with paralysis [5]. Because of the limited processing capabilities of current implantable systems and the early stage, developing nature of cortical interfacing, these recorded signals must be transmitted from the implanted device to a processing unit external to the body to be processed into a control signal. A block diagram of a generic FES system utilizing a biopotential control source and external processing unit with a telemetry link is shown in Figure 1. As shown in this figure, a biopotential control signal is recorded (e.g. from a cortical electrode array) and subsequently processed into a serial data stream. This data is transmitted across a telemetry link to an external device for processing. As shown in the figure, the telemetry link could be bidirectional, allowing for actuation information to be transmitted back to the FES system. This document presents a telemetry link specifically designed for transmitting cortical microelectrode array data from an implanted system to an external signal processor.

**Figure 1:** Block diagram of a generic FES system with a telemetry link to an external signal processing unit.



## *B. Link Design Specifications*

It is useful to present the problem of designing the link in terms of the specifications required. These specifications can be classified as functional specifications and technical specifications. The functional specifications are what are functionally required of the device. The technical specifications describe the particular operating parameters for the link that ensure that the functional specifications are met. Some of the technical specifications are particular to the telemetry modality used. For this work, optical telemetry was selected to be the best telemetry modality for this application. The reasons for choosing this modality are described in the section ‘Choosing a Method for Data Transmission,’ in this chapter.

### *1) Functional Specifications*

1. The link must be capable of transmitting data generated by a 100 channel cortical electrode array across the skin to an externally located receiver.
2. The device must not span the skin (i.e. the internal portion must be fully implanted).
3. The latency induced by the device must not interfere with the potential for real-time cortical control of a FES system.
4. The device must be capable of operating for approximately one day given a portable power supply.
5. The device must transmit the data with a quality that is sufficient for adequate detection of neural spike rates by a cortical signal processor.

6. The physical dimensions of the internal (transmitting) portion of the link must be sufficiently small for implantation.
7. The implantation procedure must utilize known surgical procedures.
8. The form and physical dimensions of the external (receiving) portion of the link must be sufficiently small such that the device is not cumbersome to use.
9. The external device must maintain sufficient cosmetic appeal such that most users would be comfortable using the device in public.
10. The device must be capable of being activated and placed into its normal operating mode by a patient's aid without difficulty.
11. The device must be capable of operation without failure for approximately 5 years.
12. The device should maintain as much manufacturability as possible.
13. Operation of the device should not pose a significant safety risk to the user.

## 2) *Technical Specifications*

1. The link must be capable of operating at a data rate of 40 Mbps.

This technical specification is dictated by Functional Specification 1. Transmitting many channels of neural waveform data across the skin requires a large communication channel bandwidth. These neurological potentials have frequency characteristics from the DC - 10 kHz range [6], and therefore need to be sampled at a rate of at least 20 kSamples/sec (commercial neural recording systems often sample at 25-30 kSamples/sec). The sample resolution will depend on the analog-to-digital converter, ADC, input range and proper amplification of the neural signal. Sampling resolutions as low as 8-bits/sample have been implemented successfully [7], although a resolution of 10

bits/sample or more may be more realistic for a robust system. Given communication overhead (protocol overhead, modulation overhead, error-correction, etc.), actual transmitted bit rates could be significantly higher than the bit rate required for data alone (e.g. 8B/10B data encoding, a commonly used method, requires a transmission bit rate that is 125% that of the data [8]). This translates into a data rate requirement of approximately 40 Mbps for a link capable of transmitting 100 channels of neural waveform data across the skin. Selecting the type of telemetry for achieving these data rates is discussed in the section titled ‘Choosing a Method for Data Transmission’, later in this chapter. A wireless modality is required to satisfy Functional Specification 2.

2. The link must not induce a data latency greater than 10 ms.

This technical specification is dictated by Functional Specification 3. The latency specification is framed around the requirement that the FES control system should be able to update a 25 Hz stimulus pulse train on a pulse-pulse basis. The inter-pulse interval at 25 Hz is 40 ms. Assuming the link can consume up to 25% of the total latency allowed, a 10 ms maximal latency is allowed for the link hardware.

3. The power consumption for the device should be below 100 mW.

This technical specification is dictated by Functional Specification 4. While it is difficult to specify a particular power consumption limit for the device, a consumption of 100 mW or less would place the device in an operating range that is realistic for operation with an implanted FES system using rechargeable batteries.

4. The maximum bit error rate at which the device should operate is  $10^{-5}$  errors/bit.

This technical specification is dictated by Functional Specification 5. The value of  $10^{-5}$  was determined by simulations that showed the tolerance of spike detection

algorithms to bit errors at this rate. These simulations are described in greater detail in Chapter 3.

5. The physical dimensions of the implanted portion of the link should be no larger than 31 mm x 25 mm x 6 mm.

This technical specification is dictated by Functional Specification 6. The two primary candidate implantation sites for the transmitting device are a cavity in the mastoid process of the temporal bone of the skull, and a subdermal cavity in the thoracic region. These two locations were chosen because they are traditional sites for the implantation of other devices: the mastoid is a common implantation site for cochlear implant receivers, and the chest is a common implantation site for cardiac pacers and deep brain stimulators. If the internal portion of the link is to be capable of implantation in the mastoid cavity, it should not exceed the dimensions of the largest commercial cochlear implant that has been implanted. The dimensions of this device are 31 mm x 25 mm x 6 mm [Clark]. Utilizing these traditional implantation sites also ensures that known surgical techniques are used, addressing Functional Specification 7.

6. The physical dimensions of the external portion of the link should be no larger than the approximate size of a behind-the-ear hearing aid.

This technical specification is dictated by Functional Specifications 8 and 9. As described in the section titled ‘Choosing a Method for Data Transmission,’ optical telemetry is the best modality for achieving wireless telemetry at the data rates required. Since optical energy is directional in nature, the transmitter and receiver must be within close proximity. If the device is to be implanted in a cavity in the mastoid process, the receiving device would be worn behind the ear. This device could be designed to look

like a standard hearing aid, a device which is used by a large percentage of the public, and would likely have reasonable cosmetic appeal. This dictates that the receiving device fit behind the ear and fit into a package that resembles an external hearing aid.

7. The link must be tolerant of at least 2 mm of transverse transmitter-receiver misalignment.

This technical specification is dictated by Functional Specification 10. An optical transmitter and receiver must have relatively intimate alignment for the receiver to collect enough transmitted light for operation, but the link must also be tolerant enough to misalignment that the receiving device can be easily placed by a clinician or patient's aid without difficulty. Allowing for a transverse transmitter-receiver misalignment of 2 mm in any direction would provide this functionality.

8. The link must utilize durable, high quality, components that are commercially available when possible.

This technical specification is dictated by Functional Specifications 11 and 12. The utilization of high quality components that are designed for long operational lifetimes will help ensure that the device lifetime requirement of approximately 5 years will be met. Utilization of commercial components will help the device maintain its potential for manufacturing.

9. The optical emitter must not expose the skin to radiation of intensity greater than that allowed by the ANSI national standards.

This technical specification is dictated by Functional Specification 13. The maximum permissible exposure levels vary with wavelength, and are explained in greater detail in the 'Optical Safety Hazards' section of this chapter.

### *C. Fundamentals of Data Transfer*

The data rate specification of 40 Mbps is quite high relative to most current transcutaneous data transmission systems, and selecting the method to best transmit this data across the skin requires knowledge of some fundamentals of data transfer.

Two factors determine the bit rate capacity of a data channel: the bandwidth, BW, and the signal to noise ratio, SNR, of the channel. The Shannon-Hartley theorem states that the maximum capacity of an information channel (with an arbitrarily low error rate) is  $C = BW * \log_2\left(1 + \frac{S}{N}\right)$  [9]. This means that BW can be traded for SNR and visa-versa when designing a telemetry link (i.e. a reduction in transmitter power for a given noise level, or a reduction in required BW for an increase in power). This tradeoff is made possible by the encoding (modulating) of the original digital data into a different signal which is transmitted through the communication channel. Work by Nyquist showed that the maximum capacity of an information channel is related to the encoding mechanism by  $C = 2BW * \log_2(M)$ , where M is the number of possible signal states per pulse [10]. In general, this means that the more signal states that are used by the encoding scheme, the more BW efficient the scheme will be, at the expense of an increased requirement in the SNR. This means that the lowest power transmission schemes will require a large bandwidth, and the most bandwidth efficient schemes will require a large SNR (and therefore transmitter power for a given noise level). Telemetry modalities can therefore be evaluated by the BW and SNR they are capable of achieving.

#### *D. Choosing a Method for Data Transmission*

Transcutaneous data transmission can be achieved via several modalities, including the use of percutaneous wires, acoustic energy and electromagnetic energy (both RF and optical). Each of these modalities was evaluated for its practicality in achieving the BW and SNR required for meeting Technical Specification 1, achieving 40 Mbps data transmission. Cosmesis and the engineering practicality of implementing each method was also evaluated, per Functional Specification 9.

Percutaneous wires (i.e. connecting the “transmitter” and “receiver” by wires that span the skin) are not considered to be a permanent long-term solution to the need for transcutaneous data transfer. With respect to BW and SNR, percutaneous wires provide a very attractive solution. Unfortunately, as suggested by Functional Specification 2, concerns of cosmesis and patient acceptance drive the need for a data channel that does not physically span the skin. Additionally, while infection rates for percutaneous wires have been shown to be low [11], a solution that does not span the skin would be ideal for minimizing infection.

Ultrasonic acoustics is a candidate technique for high data rate transcutaneous telemetry due to the large channel bandwidths possible, and has been used as a means of telemetry for cochlear implants [12]. The technique is not considered to be a viable modality for two primary reasons: 1) use of acoustics for transcutaneous telemetry is not common and is therefore poorly documented in literature, and 2) ultrasonic transducers are piezoelectric materials that tend to be driven by high voltages [13], which is not ideal for an implanted device. Poor documentation and a lack of commercially available

ultrasonic telemetry components limit the practicality of implementing a clinically robust telemetry link using this modality.

Radio (RF) telemetry (inductive and antenna coupled) is a mature, well established technology and has been used for diverse applications, including neuromuscular stimulators [14], commercial implantable cardioverter defibrillators and commercial cochlear implants for many years. Neural microelectrode recording systems with integrated RF telemetry systems are also being developed [15]-[17]. The primary advantage of RF telemetry systems over other methods of telemetry is the potential transmitter-receiver separation achievable by some of these systems, a distinct advantage with respect to device cosmesis. Current systems have been shown to be capable of data rates of up to several Mbps [15]. Unfortunately, RF telemetry has some major disadvantages with respect to achieving a sufficient BW and SNR for operation at high data rates. Radio bandwidth is firmly regulated by the Federal Communications Commission (FCC), limiting the options for high bandwidth systems. Frequency bands that can legally be utilized by a medical telemetry device are limited to the Medical Implants Communication Service (MICS) band (402-405 MHz) and the Industrial, Scientific and Medical bands (ISM) [18]. Of the available frequency bands, only a few are realistic candidates for high data rate transcutaneous communication: 902 – 928 MHz, 2.4 – 2.5 GHz and 5.725 – 5.875 GHz. These frequency bands are becoming increasingly crowded because of commonly used wireless communication protocols such as 802.11, Bluetooth, and others. Since the bandwidth is limited, RF telemetry links often take advantage of the Nyquist relationship described above, and utilize multiple encoding states. A higher SNR is required for these systems that utilize a large number of signal

states than for those using a simpler binary encoding scheme. This often translates into high power consumption for large bit rates.

RF systems also have disadvantages with respect to achieving a SNR sufficient for operation. The SNR for a radio telemetry link is limited by a number of factors including the transmitter power, inherent electrical noise sources, tissue absorption of the carrier, interfering noise from other RF sources (e.g. wireless network users, wireless telephones, etc.) and the location and separation of the transmitter and receiver. Devices operating outside of the MICS or ISM bands must operate at very low power levels (as mandated by the FCC), making them even more susceptible to interference from other sources. Absorption of the carrier signal by the tissue may also be a significant contributing factor, and increases with the square of the frequency [19], resulting in a decreased signal to noise ratio for a given power budget when higher frequencies are used (the higher BW bands are at higher frequencies). While transcutaneous RF data transmission that meets the 40 Mbps specification is likely technically possible, it would be quite difficult to achieve a practical system because of the reasons described above.

Optical telemetry is also a mature, well established technology: fiber-optic and free-air optical communication systems are common in consumer goods and are quite well understood. Optical telemetry offers two significant advantages that make it quite attractive for high rate biotelemetry: the optical portion of the EM spectrum is unregulated worldwide for communications purposes, and interference from other sources is inherently minor (due to the line-of-site nature of optical telemetry), and can be further reduced with filtering (described in greater detail below). Since the optical spectrum is unregulated, the bandwidth for an optical transcutaneous telemetry link is

limited only by the bandwidth of the transmitting and receiving electronics, and the scattering effects of the skin. Based on the preliminary photon spread data published by Eigensee, et. al. [20], the scattering effects of the skin on bandwidth are negligible at the data rates of interest, and should allow for data rates as high as 100s of Gbps before multipath distortion begins to significantly affect data transmission (multipath distortion is further explained below) [21]. Additionally, data is modulated using Intensity Modulation with Direct Detection, IM/DD, a method where the intensity of the optical field is converted directly into a photocurrent that is proportional to the field power [22],[23]. This allows for simple modulation and demodulation with straightforward circuitry (data modulation is discussed in further detail below). In transcutaneous optical telemetry, binary modulation is almost always preferred, as it takes advantage of the enormous bandwidth available in favor of power conservation (effectively only using two signal states: zero power, and the lowest reasonably detected power level). The very large available bandwidth, the lack of interfering sources, and the ease of modulation and demodulation makes optical telemetry quite suitable for transcutaneous data transfer.

Optical telemetry has been used for several transcutaneous communication applications. Low to moderate data rate (9.6 kbps – 1 Mbps) implementations include systems for providing command signals or low rate data to or from neuromuscular stimulators [24], artificial hearts or implanted cardiac assist devices [25]-[27], bladder stimulators [28], laboratory animal monitoring systems [29], neural recording systems [30],[31] and generic communication systems [32]. A higher rate implementation has also been developed, showing the feasibility of high rate optical transcutaneous data transfer at rates of 10-80 Mbps [33]. This high rate system required relatively large

amounts of power to perform successfully (30-40 mW emitter consumption @ 40 Mbps [33]), which would limit the applicability of an optical link for an implanted system. The work presented in this document shows that a knowledge of how to effectively design the interface between the transmitter, receiver and the skin can allow for an optical link that operates at a much lower power (4.3 mW at 40 Mbps).

Given the inherent advantages with respect to bandwidth, interfering noise and simplicity of modulation, optical telemetry is the most ideal of the evaluated modalities for high speed transcutaneous data transmission. Additionally, the technology for implementing such a system is mature, and the associated electronic components are widely available in the commercial marketplace (which is important for satisfying Functional Specifications 11 and 12). In summary, optical telemetry is the best choice of the evaluated modalities for satisfying the functional and technical specifications described above.

#### *E. Fundamentals of Optical Communication*

Optical telemetry was chosen to be the most ideal modality for constructing a telemetry link that satisfies the design specifications. The transcutaneous optical telemetry link, TOTL, that was constructed for this work leveraged many techniques and components common to other optical communication systems (both fiber-optic and free air infrared systems). Most of the fundamental principles of operation for these systems are similar, only the transmission medium changes (e.g. a fiber, a room, skin). Therefore, it is important to understand these principles in order to properly design a TOTL. Many

of these principles and their specific relevance to transcutaneous systems are described below.

*1) Optical Transmitters*

Semiconductor photoemitters convert an electrical signal into an optical signal. Common emitters include the light emitting diode, LED, the laser diode, LD, and the vertical cavity surface emitting laser, VCSEL. Communication systems which use each of these emitters exist, and each has its own characteristics.

The LED is commonly used in the wireless IR communication industry, primarily due to its wide availability, low cost, reasonable power consumption and relatively low risk to safety [23,34]. These attributes also make the LED attractive for use in a transcutaneous system. Unfortunately, LEDs generally have a poor electrical-optical power efficiency, limiting their applicability for a TOTL [23].

Laser diodes have a very narrow optical bandwidth ( $\sim 1$  nm), and tend to have higher performance than LEDs with respect to electrical-optical power efficiency and wide modulation bandwidths [23]. While laser diodes would be appropriate for transcutaneous data transfer, they are less power efficient than vertical cavity surface emitting lasers, VCSELs.

VCSELs are also narrow-band emitters, and essentially represent a paradigm shift in power efficiency over LEDs and laser diodes. VCSELs tend to have very large modulation bandwidths, and are becoming very common in fiber optic systems. The major deficits of the technology are cost, availability and wavelength diversity (VCSEL technology is relatively young, and few wavelengths are available). Fortunately, 850 nm VCSELs are fairly ubiquitous, a wavelength that is suitable for transcutaneous communication (wavelength selection is described below). This power efficiency, wide

bandwidth and near-infrared wavelength availability make VCSEL technology an obvious choice for transcutaneous telemetry, and help to ensure that Technical Specifications 1,3 and 8 are satisfied. This is the technology chosen for the link described in this work.

## 2) *Optical Detectors*

Semiconductor photodetectors convert an optical signal into an electrical signal. There are a multitude of photodetectors used in optical communication, including the p-n photodiode, the p-i-n photodiode, the metal-semiconductor photodiode and the avalanche photodiode [35]. Both the p-i-n photodiode and the avalanche photodiode, APD, are used in common optical communication systems [23,36].

APDs have an intrinsic gain and are quite sensitive to incident light, allowing for low power transmitters [23]. This sensitivity comes at the expense of necessarily low ambient light levels (as this noise is also amplified) and an extremely high reverse-bias voltage (as high as  $\sim 100$  V -  $\sim 2,000$  V depending on the device and desired gain) [35]. APDs may also require cooling. Because of the high bias voltage and potential cooling requirements, most avalanche photodiodes are not practical for transcutaneous biotelemetry.

The photodetector most commonly used for optical communications is the p-i-n photodiode. These photodiodes are generally inexpensive, are available with a large optically responsive area, tend to have natural optical bandpass characteristics and generally have a high quantum efficiency (ratio of electrical carriers generated to the number of incident photons – directly related to the responsivity,  $R$ , or photodiode gain) [23]. For these reasons, a p-i-n photodiode was chosen for the TOTL described in this work. In

general, the photodiode selected for a TOTL should have a bandwidth sufficient for the data rate needed, should have a high responsivity and a large active area.

### 3) *Optics and Filtering*

To optimize optical coupling efficiency of the transmitter and receiver, and to minimize noise resulting from ambient light sources, a lens and/or optical filter can be placed in front of the photodiode. Such filters and lenses can often be found integrated with many commercially available photodetectors. Optical filters generally exert a bandpass or longpass filtering effect on incident light. This reduces the intensity of light residing outside of the spectral band native to the photoemitter – (i.e. that of the noise) that reaches the detector. A longpass filter, (a high or low pass filter), can be used in conjunction with a photodetector's natural highpass or lowpass cutoff characteristics to generate a bandpass filter that is appropriately matched to the emission spectrum of the photoemitter. [23]

The optics system employed in the link design is quite important. It will help dictate the amount of signal power collected by the receiver, and therefore the dynamics of the power consumption/data quality tradeoff for the link. Various optics systems can be utilized for collecting transmitted light and focusing it on the photodiode. These systems include imaging optics, non-imaging lenses and fiber-optic tapers. The link constructed for this work utilizes a simple non-imaging lens that is integrated with the photodiode. This configuration is simple, is physically small and provides a reasonable enhancement of light collection over the bare photodiode. The specific optics configuration used was selected to ensure proper receiver SNR (and therefore satisfaction of Technical Specifications 1,3 and 4), and appropriateness of the physical form (and therefore

satisfaction of Technical Specifications 5,6 and 7). This configuration and its effects on the receiver SNR are further discussed in Chapters 2 and 3.

#### 4) *Transmission Medium and Transmitter-Receiver Alignment*

With the exception of a complete vacuum, any medium through which light propagates absorbs and scatters photons. For skin, these absorption and scattering effects are quite significant and act to disperse the optical signal on the epidermal surface of the skin (assuming data is being transmitted from the inside to the outside of the body). As described in detail in Chapter 2, these effects vary significantly with the thickness of the skin and played a very significant role in the design of the telemetry link, particularly with respect to satisfying Technical Specification 7 (a transmitter-receiver misalignment tolerance of 2 mm)

Due to the directional nature of light propagation, the transmitter and receiver must be intimately aligned for efficient power transfer in a TOTL. The degree to which they are misaligned affects the amount of power transferred (more misalignment results in less signal power transfer, and therefore a lower SNR). Designing a system that is tolerant to some misalignment is important. As described above, the external unit will likely be placed by a patient's aid, and it is unrealistic to expect perfect placement. Chapter 2 describes experiments that were performed to determine the effects of misalignment on the efficiency of signal power transfer. A link's tolerance to misalignment can be increased by two methods: increasing the transmitter power (so that sufficient power reaches the receiver even when it is aligned at the periphery of the transmission field), and using a larger lens (so that light from the central region of the transmission field is still collected despite the misalignment). Each of these design parameters affects the others, and a system that best satisfies the technical and functional specifications must be

chosen. The precise way the design parameters interact is described in greater detail in Chapter 2.

##### 5) *Noise in Optical Communication Systems*

As mentioned in the above section on Fundamentals of Data Transfer, the signal-to-noise ratio, SNR, of the receiver dictates the quality and rate of data that can be transmitted across the link. Receiver noise is the result of two fundamental noise sources: electrical noise and noise resulting from ambient light striking the photodiode. Mitigating noise from these sources is important for achieving low power transmission, because more signal power is required to compensate for noise when a certain SNR is required. Noise levels therefore affect the ability for the link to satisfy Technical Specifications 1,3,4 and 7.

Electrical noise has contributions from several sources, including shot noise and thermal noise [23],[35]. Shot noise is the result of the random nature of photocurrent electron generation. Shot noise can be approximated as white and Gaussian, with a spectral density,  $S(f)$ , that is proportional to the incident light power as,

$$S(f) = qRP$$

where  $q$  is the charge on an electron,  $R$  is the detector responsivity and  $P$  is the incident optical power [36]. This dependence on the incident light power implies that shot noise is most significant when there is intense ambient light. For systems which operate with their receivers exposed to large amounts of ambient light, shot noise is the predominant noise source [23]. Shot noise induced by ambient light can be reduced by using optical filters. If optical filters are used, ambient light and therefore shot noise may be kept to a minimum. An optical filter is used in the link described in this work. The specific effects of filtering on ambient light noise are discussed in greater detail in Chapter 3.

Thermal noise, aka ‘Johnson’ or ‘Nyquist’ noise, in the receiver circuit can also be a significant contributor to total noise. Thermal noise arises from random electron movement that occurs in any conductor with a temperature above absolute zero. The primary circuit components contributing to the overall thermal noise are the feedback/load resistance and the transistors in the amplification circuitry. Transistor noise is dependent on the signal frequency and is more significant for higher bit rate systems (utilizing higher frequencies). It can also be reduced by choosing ICs with high  $g_m$  transistors and a receiving photodiode with a low capacitance. Many low noise commercial, off-the-shelf, OTS, transimpedance preamplifiers are available, which makes low noise receiver design quite manageable. [23,36] Such a device was chosen as the preamplifier for this link, and is described in Chapter 3.

Ambient light sources can induce both DC and periodic noise in optical receiver systems. The three primary ambient light sources are sunlight, incandescent lighting and fluorescent lighting [37]. Sunlight induces a DC noise signal with a maximum power density at a wavelength of approximately 500 nm and minimums in the NIR region at 1100 nm and 1400 nm [38]. Incandescent lights induce a periodic noise signal on optical receivers, emitting light of significant power at harmonics in the kHz range (discussed in greater detail in Chapter 3). Given the range of operating locations for a clinically relevant TOTL, each of these emitters are potential noise sources.

The link constructed for this work utilizes both a signal domain and an optical domain filter to mitigate the effects of ambient light noise. Experiments that examined the effect of the specific filters used on the relative magnitude of ambient light noise seen by the receiver are described in detail in Chapter 3. Additionally, by placing the receiver in

direct contact with the patient's skin, much of the ambient light may be shielded from ever reaching the detector. A low noise preamplifier was chosen to minimize Johnson noise.

6) *Multipath Distortion: Intersymbol Interference (ISI)*

Multipath distortion is the spread of a signal in the time domain due to light waves arriving at the detector at slightly different times. This occurs when reflection or scattering causes the propagating light waves to travel multiple paths of varying length to the detector. This phenomenon results in the "spreading" of signals in the time domain, effectively limiting the bandwidth of the signal [21]. If the spread is significant enough, correct identification of a digital bit becomes difficult. This problem is especially relevant for free-air systems, where widely varying photon path-lengths exist [21]. Based on the preliminary photon spread data published by Eigensee, et. al. [20], the scattering effects of the skin on bandwidth are negligible at the data rates of interest, and should allow for data rates as high as 100s of Gbps before multipath distortion begins to significantly affect data transmission.

F. *Optical Properties of Skin*

As discussed above, the SNR at the receiver is quite important for achieving quality data transmission at the 40 Mbps required, at a reasonable power level (less than 100 mW). The optical properties of the skin through which data is being transmitted greatly effect the distribution of the light on the receiving surface, and therefore how much signal-producing light is collected by the receiver. An understanding of these optical properties is important to an understanding of how light is distributed. Chapter 2 describes experiments and a detailed analysis of how these properties affect the SNR at

the receiver. These studies demonstrated how the various design parameters can be manipulated to achieve a receiver design that meets the technical specifications. Below is a discussion of the nature of human skin, the major factors that affect the way light is transmitted through it and how these properties affect the design of a TOTL.

*1) The Layers of Human Skin*

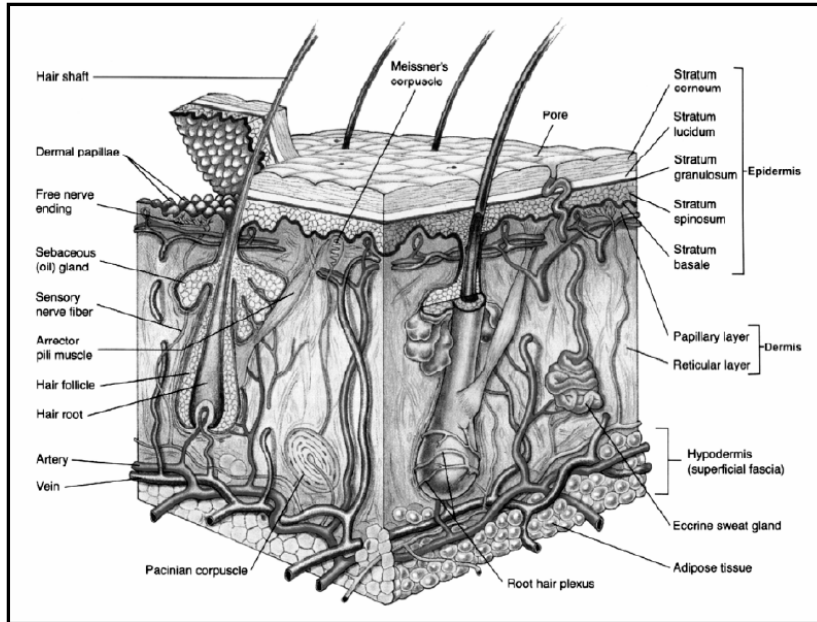
Human cutis consists of two primary layers, the epidermis and the dermis. Both the epidermis and the dermis are further subdivided into layers. As shown in Figure 2, the epidermis consists of the stratum corneum and four other layers, the stratum lucidum, the stratum granulosum, the stratum spinosum and the stratum basale. The dermis consists of two layers, the papillary dermis and the reticular dermis. Below the dermis is the hypodermis or subcutis, consisting of the fascia and adipose tissue. [39] It is this hypodermal layer that contributes the most to the varying “skin” thickness. Experiments evaluating the specific effects of this thickness on the design of the transmitter-skin-receiver interface, and the performance of the TOTL are described in Chapters 2 and 3, respectively.

*2) The UV, Visible and IR spectrum*

While there are no strict wavelength boundaries for separating the UV, Visible and IR portions of the spectrum, there are generally accepted regions for differentiation. The UV band is generally held to be from approximately 10 nm – 390 nm, the visible band is generally held to be from approximately 390 nm – 780 nm and the infrared band is generally held to be from approximately 800 nm – 1 mm. The near-infrared, NIR, band is the band of infrared light with the shortest wavelengths, ~800 nm - ~2200 nm, that is, those wavelengths ‘nearest’ to the visible band. Chromophores (proteins,

**Figure 2:** The layers of human skin. Reprinted from

Marieb EN. *Human Anatomy and Physiology*. Third Edition. 1995. Redwood City, CA: Benjamin/Cummings.



molecules or chemical residues that absorb light) in human skin absorb and scatter light in each of these wavelength bands.

### 3) *Chromophores*

There are seven relevant chromophores in the human skin that absorb in the visible and/or near-infrared spectrum: eumelanin, pheomelanin, bilirubin, oxyhemoglobin, deoxyhemoglobin,  $\beta$ -carotene and water [40],[41]. The dermal layers in which these chromophores reside, the relevant bands in which they absorb and the relevant peak absorption wavelength(s) for each are listed in Table 1, and are shown in Figure 3 [40]-[42].

There are significant variations in dermal chromophore concentrations within the human population [43], resulting in light absorption characteristics that vary with skin pigmentation in the visible and UV portion of the spectrum [42]. This effect lessens with an increase in wavelength since these chromophores tend to have a higher absorption coefficient for shorter wavelengths of light (the absorptive properties of some of these chromophores at the shorter wavelengths serves to protect the body from ionizing radiation). Light absorption in the near-infrared (NIR) band is primarily due to water and oxy-/deoxyhemoglobin, and is therefore nearly identical for skin types of varying pigmentation [42].

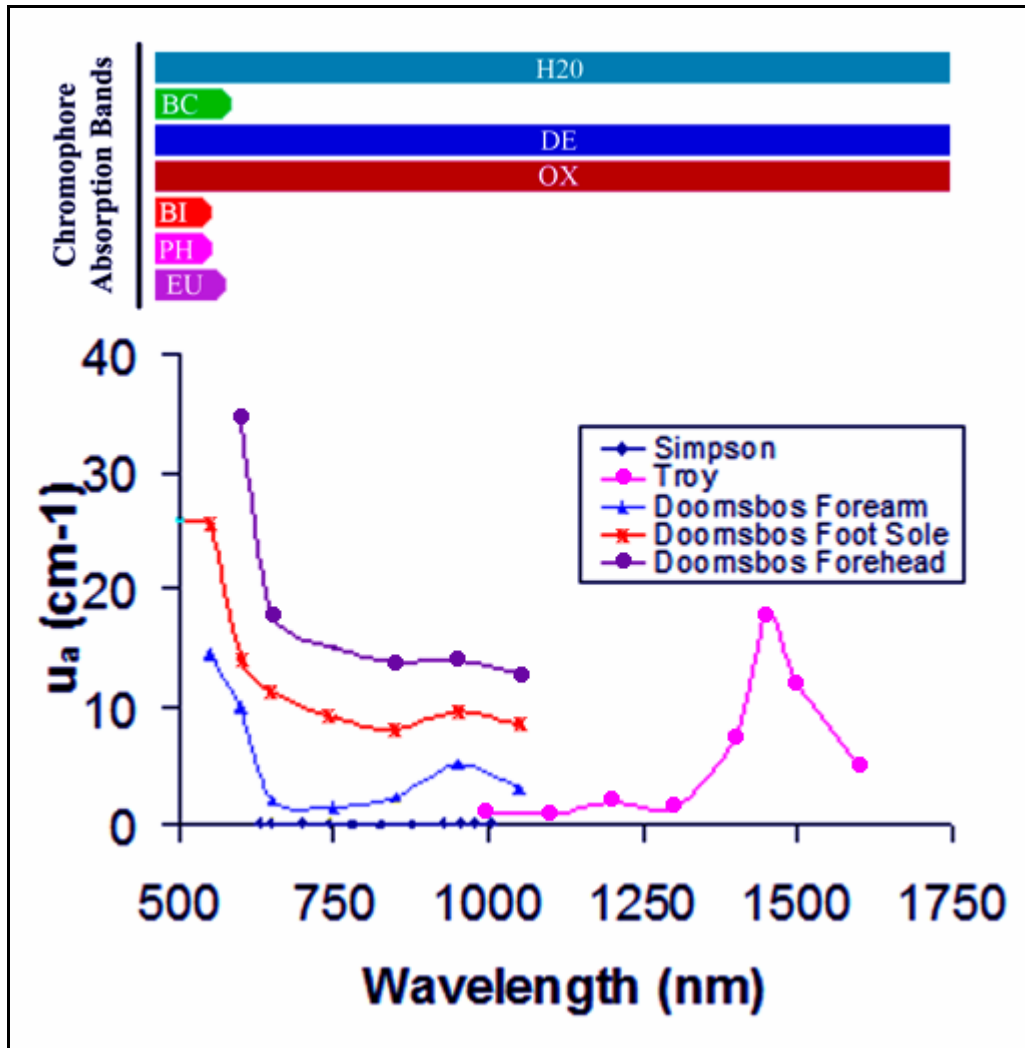
### 4) *Light Propagation in Human Skin*

Skin is a turbid material, meaning that as photons travel through the skin, they are both absorbed and scattered by elements in the skin. The absorptive and scattering properties of skin (and other materials) can be quantified by the absorption coefficient,  $\mu_a$  ( $\text{cm}^{-1}$ ) and the reduced scattering coefficient,  $\mu_s'$  ( $\text{cm}^{-1}$ ), respectively.

**Table 1:** Chromophores, their layer of origin, absorption band and peak absorption wavelength. Data for wavelengths < 400 nm is not considered. [40]-[42] Parenthetic abbreviations correspond to the bands in Figure 3.

<b>Chromophore</b>	<b>Dermal Layer</b>	<b>Absorption Band</b>	<b>Peak Absorption</b>
eumelanin (EU)	Epidermis	$\leq 600$ nm	< 400 nm
phaeomelanin (PH)	Epidermis	$\leq 500$ nm	< 400 nm
bilirubin (BI)	Dermis	350 – 500 nm	450 nm
oxyhemoglobin (OX)	Dermis	$\leq 450, 500 - 600$ nm, N	415 nm, 540 nm, 580 nm
deoxyhemoglobin (D)	Dermis	$\leq 450, 500 - 600$ nm, N	440 nm, 555 nm
$\beta$ -carotene (BC)	Dermis & Epidermis	$\leq 500$ nm	455 nm
water (H <sub>2</sub> O)	Throughout	$\geq 900$ nm	965 nm, 1450 nm

**Figure 3:** The absorption coefficients for human skin, as reprinted from [42],[45],[46]. Bars at the top of the figure show chromophore absorption bands, as described in Table 1.

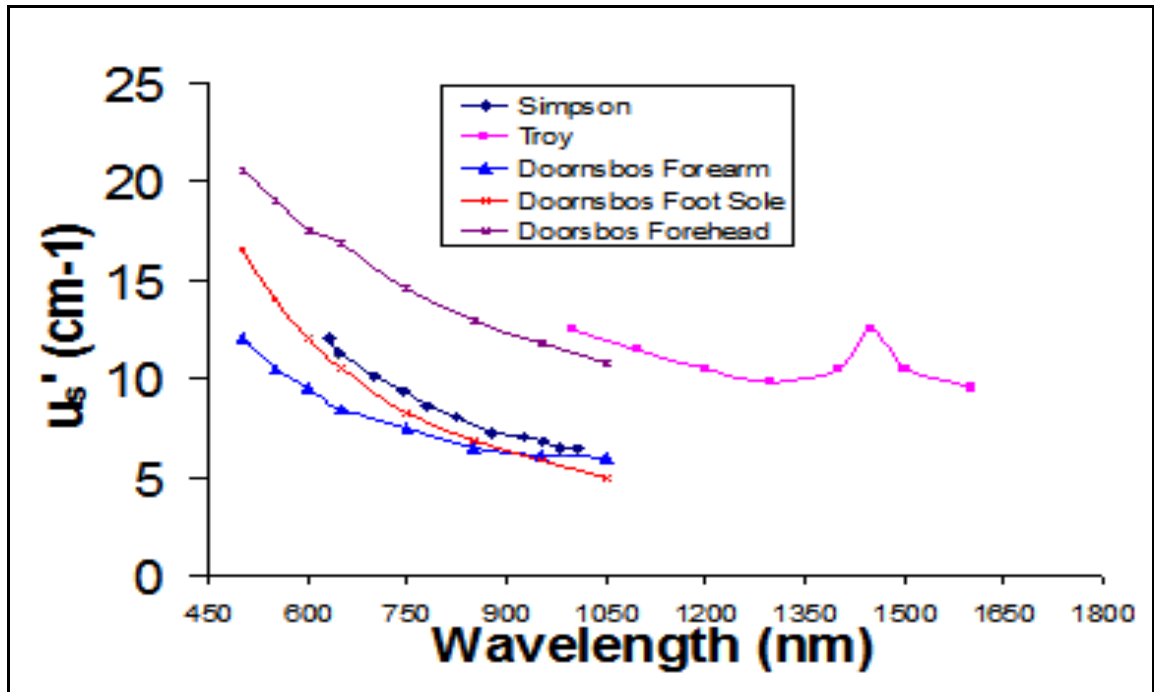


Skin's scattering and absorptive properties are wavelength and chromophore concentration dependent. Absorption due to the presence of chromophores is most apparent in the ultraviolet band and the shorter wavelengths of the visible band [44]. Skin with a high concentration of melanin also has significant absorption in the visible band [42]. Absorption of light in the NIR band is mostly attributed to water, which has absorption peaks at 965 nm and 1450 nm, and oxy-/deoxyhemoglobin. [41],[45]-[47]. The overall absorption trends can be seen in Figure 3, as replotted from [42],[45],[46]. The higher the absorption coefficient, the more light is absorbed by the skin, and the less efficient the signal power transfer will be (i.e. more transmitter power will be required to achieve the same SNR). The data from the three studies does not integrate perfectly, because the skin samples in each study were from different parts of the body and were analyzed under different circumstances, using different methods.

Scattering is also an important factor in determining how the transmitted light will be distributed on the receiving surface of the skin. A larger scattering coefficient results in a wider power distribution, and also results in lower signal power transmission efficiencies (scattered photons travel longer paths and therefore have a greater probability of being absorbed). The reduced scattering coefficient is a function that describes the degree of both surface and subsurface scattering of the skin [40]. The overall scattering trends can be seen in Figure 4, as replotted from [42],[45],[46]. Like the absorption data, the scattering data from the three studies does not integrate perfectly.

The trend shown in Figures 3 and 4 suggests that there is an optimal range for efficient operation of a transcutaneous optical telemetry link: ~750nm to ~1300nm. A transmitter wavelength of 850 nm was chosen for this TOTL, as described in Chapter 3.

**Figure 4:** The reduced scattering coefficients for human skin as replotted from [42],[45],[46].



This wavelength is within this optimal range, and is also a wavelength at which efficient VCSELs are manufactured. Operation at this wavelength ensures the highest power efficiency possible, helping ensure the satisfaction of the power requirements laid out in Technical Specification 3.

#### 5) *Optical Clearing*

Optical clearing is a method for reducing the scattering effects of skin by using hyperosmotic agents on the skin's surface. This method could potentially be used to increase the power efficiency of a TOTL [48],[49]. Optical clearing reduces scatter via two mechanisms:

1. The refractive index of the chemical agent is matched to that of the main constituents of the tissue [48]
2. The tissue is dehydrated, compacting the scattering elements in the tissue [48]

Increases in transmittance of up to 100 % have been realized using glycerol *in vitro*, and increases in transmittance of up to 250 % have been realized using DMSO (dimethyl sulfoxide) *in vitro* [49]. Use of these agents is likely not practical for daily use, although they could play a role as a diagnostic tool for troubleshooting link failure in a clinical setting.

#### G. *Optical Safety Hazards*

Transmitting light through skin, even at its most transmissive wavelengths, can potentially pose two primary safety hazards: irradiative heating, and conductive heating. The design of a TOTL must take these risks into account, and must be designed to ensure user safety, per Functional Specification 13 and Technical Specification 9.

### 1) *Irradiative Heating*

Irradiative heating, or heating by absorption of light, has been shown to increase dermal temperature, which can be a hazard if the temperature becomes excessive [50],[51]. Cells sustained at a temperature above 41 °C for extended periods of time have an increased likelihood of cell death [50]. IEC standard 60601 states that cells may safely sustain temperatures of 43 °C for four hours or less, 42 °C for eight hours or less and 41 °C for extended periods of time [52]. Skin temperature varies significantly as a function of anatomical location, resulting in different permissible temperature increases depending on the location of the radiation. For example, the average temperature of skin on the arm is 32 °C and the average temperature of the forehead is 35 °C [51]. A TOTL should therefore limit radiation such that no temperature increases beyond 41 °C occur.

The American National Standard Institute, ANSI, defines maximum permissible exposure, MPE, limits, defining maximum power densities and exposure times for preventing skin damage (i.e. temperature increases above 41° C) as a result of NIR light exposure. The ANSI Z136.1 standard provides MPE levels for human skin over a variety of different wavelength ranges. The standard provides equations for calculating the MPE for continuous wave exposure for 10 sec – 30,000 sec (8 hours 20 min). These maximum exposure levels (for the NIR wavelength range of interest) are shown in Figure 5. The standard sets a ceiling level of 1 W/cm<sup>2</sup> that applies regardless of wavelength. The TOTL designed for this work uses a VCSEL operating at 850 nm, a wavelength at which a MPE of 450 mW/cm<sup>2</sup> is permitted by the standard. For reference, the total NIR spectrum exposure to skin in direct sunlight is approximately 50 mW/cm<sup>2</sup> [51].

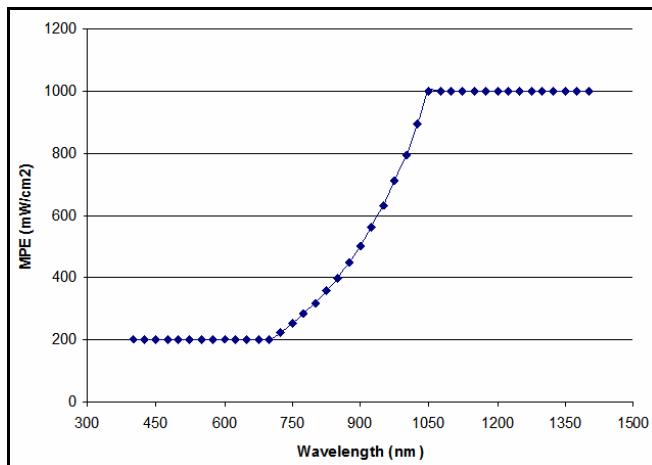
ANSI MPE values are meant to be a blanket reference that will provide safety for most reasonable operating conditions, and as a result provide a large margin of safety for

some anomalous operating conditions such as having a small exposure area. [53] For example: NIR absorption at 789 nm has been shown to heat skin tissue *in vivo* at 0.101 °C/mW of total laser diode power using a 1 mm diameter optical fiber to direct light from the diode to the skin [50]. Assuming a conservative 37 °C arm temperature, for a safety margin of 4 °C (maximum skin temperature of 41 °C), a source intensity of 5,600 mW/cm<sup>2</sup> could be safely used on the skin (assuming conditions identical to those used by Ito et al) [50]. This is far above the ANSI MPE for 798 nm of approximately 316 mW/cm<sup>2</sup>. This implies that exposure levels larger than those permitted by the ANSI standard may be safe for use with a TOTL because of its small exposure area. The link constructed for this work operates below the ANSI MPE levels (as discussed in Chapter 3), but this idea could have important implications for devices transmitting data through very thick skin, where more transmitter power is required. Additionally, repeatedly pulsed light (which would be used for a TOTL) has been shown to produce a temperature increase that is significantly lower than the increase produced by continuous wave exposure [51].

## 2) *Conductive Heating*

When an emitter is in direct contact with human skin, conduction heating as a result of a high junction temperature has been shown to be a very significant source of heat transfer from the emitter to the skin [51]. To avoid optical output limitations as a result of conductive heating, the emitter junction (like any semiconductor device carrying a significant current) should not be placed in direct contact with the skin.

**Figure 5:** MPE for continuous wave exposure, 10 sec – 30,000 sec, in the NIR spectrum [53]. The line marks the wavelength used for the TOTL presented in this document, 850 nm.



## *H. Conclusions*

Functional design specifications have been determined for a transcutaneous link which can transmit cortical array data across the skin. These functional specifications were translated into specific technical design specifications for the optical hardware link that was ultimately built for this work. Optical telemetry was chosen to be the best method for transmitting the 40 Mbps of data specified. Optical telemetry provides significant advantages with respect to bandwidth, interfering noise and simplicity of modulation over the other methods evaluated. The optical transcutaneous data link constructed for this work (described in Chapter 3) leveraged many principles of operation common to both fiber-optic and free-air optical communication links (much of the transmitter, and receiver design). While it utilizes similar electronics hardware, using skin as a transmission medium makes transcutaneous optical telemetry fundamentally different from the other forms of optical telemetry. The transmitter-skin-receiver interface is an area of great interest, and its design is integral to achieving a SNR that is sufficient for link operation (and therefore has profound implications for satisfying the technical specifications). The tissue properties, the degree of transmitter-receiver misalignment and the optics configuration used will all affect the SNR achieved at the receiver. These effects and their implications for the design of the TOTL are discussed in detail in Chapter 2. Chapter 3 will discuss the link that was constructed based on the guidelines that resulted from the analysis in Chapter 2. Chapter 3 will also compare the actual link performance with the technical specifications described above. Chapter 4 will discuss the steps needed for a practical clinical implementation of the device.

**CHAPTER II: PAPER ONE, DESIGNING THE OPTICAL  
INTERFACE OF A TRANSCUTANEOUS OPTICAL  
TELEMETRY LINK**

## Chapter II, In Summary

In summary, the major findings from the work for Chapter II are:

- Optical telemetry shows promise for high speed transcutaneous telemetry.
- The design of the optical interface is important and has profound effects on how the technical design specifications are met.
- The optical interface design parameters can be manipulated to optimize system-level design constraints, such as a particular implant location, low power consumption, susceptibility to receiver-transmitter alignment and external device size.
- A mathematical analysis showed that the interaction between the optical interface design parameters can be shown through the receiver SNR:

$$SNR_i = \frac{I_s}{I_N} = \frac{P_s R}{I_{N_{elec}} + P_{N_{amb}} R}$$

- The received signal power is defined by:

$$P_s = \int_A [ |P_{TX}| \times J_{Rx\lambda} \times \eta_{opt} ] dA$$

The particular design parameters are shown relative to their respective variables in the equation.

- Experiments were performed to determine  $J_{Rx}$ , the flux distribution of optical power on the receiving surface of the skin.

- Increased tissue thickness causes greater absorption and scatter of photons, resulting in decreased power transmitted through the tissue and a widening of the flux distributions.
- The analysis of the parameter effects on the collected signal power demonstrated that there is an optimal point of operation for the link system, where signal power is optimized for minimal costs.

## Designing the Optical Interface of a Transcutaneous Optical Telemetry Link

### Authors (in order of appearance):

Ackermann, Jr., D. Michael<sup>1</sup>  
Smith, Brian<sup>1</sup>  
Kilgore, Kevin L.<sup>2,1,3</sup>  
Peckham, P. Hunter<sup>1,3,2</sup>  
Wang, Xiaofeng<sup>4,1</sup>

### Affiliations for each author, as indicated by footnote:

<sup>1</sup> Case Western Reserve University, Cleveland, OH, USA

<sup>2</sup> MetroHealth Medical Center, Cleveland, OH, USA

<sup>3</sup> Louis Stokes Veterans Affairs Medical Center, Cleveland, OH, USA

<sup>4</sup> The Cleveland Clinic

### Mailing Address for all authors:

Cleveland FES Center  
Hamann 601  
2500 MetroHealth Drive  
Cleveland, OH 44109

### Corresponding Author:

D. Michael Ackermann  
Case Western Reserve University  
10900 Euclid Ave.  
Wickenden Bldg. #313  
Cleveland, OH 44113  
Phone: 216-368-2948  
Fax: 216-368-4969

\*\*\*\*\*

For submission to:  
IEEE Transactions on Biomedical Engineering

## CHAPTER II: DESIGNING THE OPTICAL INTERFACE OF A TRANSCUTANEOUS OPTICAL TELEMETRY LINK

### *A. Abstract*

This chapter is a stand-alone paper that describes the transmitter-skin-receiver interface of a transcutaneous optical telemetry link. It discusses how the design parameters for this interface affect the SNR of the link receiver. The design of this link interface is important for achieving device operation that satisfies the required technical specifications established in Chapter 1. The following technical specifications are particularly relevant, as they directly affect or are directly affected by the receiver SNR: the data rate (Technical Specification 1), the power consumption (Technical Specification 3), the maximum allowed bit-error rate (Technical Specification 4), the physical dimensions of both the transmitter and receiver (Technical Specifications 5 and 6) and the transmitter-receiver misalignment tolerance (Technical Specification 7). This paper describes a mathematical analysis (and some experiments for supporting data) that quantitatively describes the relationship between some of the interface design parameters. These parameters include the thickness of the skin through which the light is transmitted, the size of the optics integration area, the degree of transmitter-receiver misalignment, the efficiency of the optics system and the emitter power. The particular combination of these parameters chosen for the hardware device (the ‘operating point’ of the link), will have profound implications for how the technical specifications are met. This paper demonstrates some of the tradeoffs involved in the selection of these design parameters.

## *B. Introduction*

Cortical interfacing is a rapidly advancing field that is showing great promise for the rehabilitation of the mobility impaired, among other applications. Recent work has shown that real-time control of computer cursors or robotic arms is possible by the actuation of recorded neural signals [1]-[4]. Currently, cortical interfacing systems (such as the Cyberkinetics Neurotechnology, Inc. BrainGate system) utilize percutaneous connectors to transmit the large amounts of neural waveform data from the implanted array to external signal processors. The practical integration of cortical interfacing into clinically relevant systems (such as motor neural prostheses [5]) will ultimately require a data transmission system that eliminates the wires and connectors which cross the skin. Optical telemetry may provide the best solution for achieving such a telemetry system, due to the large bandwidths possible and the relative noise immunity associated with optical communication.

Optical transmission has been shown to be an effective modality for transcutaneous data transfer for several implanted device systems, and has been used for many applications including neuromuscular stimulation systems [6], implanted cardiac assist devices [7]-[9], bladder stimulators [10], laboratory animal monitoring systems [11], neural recording systems [12],[13] and generic communication systems [14],[15]. While transmitter and receiver design for these systems is quite similar to fiber-optic or free air infrared links, the transmission medium is fundamentally different (skin).

When light is transmitted through skin, it is absorbed and scattered. This results in a non-uniform power distribution on the receiving surface of the skin. The receiver must be designed to collect enough of this light to reconstruct an error-free data stream. This

paper describes a detailed analysis of the transmitter-skin-receiver interface (the “optical interface”), and demonstrates how this analysis can be used to design an optical telemetry link. It will be shown that the optical interface can be designed to optimize certain system-level design constraints/specifications, including power consumption, implant location, susceptibility to transmitter-receiver misalignment and external device size.

To perform this analysis, knowledge of the pattern of light transmission that results on the receiving surface of the skin is required. Brief descriptions of distribution shape for rat skin [11] and porcine skin [14] have been published previously, but are not sufficient for quantitative analysis. For this study, light transmission profiles were empirically measured for porcine skin samples of various thicknesses. Porcine skin was determined to be a sufficient model of human skin since the optical properties of each are similar: the absorption coefficient,  $\mu_a$ , for each has been shown to be approximately  $0.05 \text{ mm}^{-1}$ , and the transport scattering coefficient,  $\mu_s'$ , has been shown to be approximately  $1.6\text{-}2.3 \text{ mm}^{-1}$  and approximately  $2.8 \text{ mm}^{-1}$  for human and porcine skin, respectively [16],[17]. The samples were illuminated from the hypodermal surface by a narrow-band emitter. Since the emitter used is a power-efficient communications grade emitter, this analysis is considered to be particularly relevant.

These empirically measured profiles were used to determine the quantitative tradeoffs between the optical interface design parameters. These parameters include: the emitter power, the skin thickness, the degree of transmitter-receiver misalignment, and the area over which the optics integrate the transmitted light. This quantitative analysis of the optical interface will allow for an optimized optical link design that is guided by an a priori assessment of these parameters.

### *C. Experimental Methods*

#### *1) Tissue Preparation*

Dermal samples, approximately 5cm x 5cm in size, of various natural thicknesses were removed from the hide of five Yorkshire-cross farm pigs within 12 hours post-mortem. The samples were cleaned with saline, and waxed and/or shaved to remove the hair. All samples were composed of epidermal and dermal layers (combined thickness of approximately 2 mm) and hypodermal/adipose layers of varying thickness (0 mm to approximately 9.5 mm thick). The total sample thickness was measured by laying the sample flat on a horizontal surface (without any tension or compression), and taken to be the gap distance between the surface and a plate lowered towards the sample until it just touched the skin surface.

#### *2) Measurement Technique*

The distribution of the transmitted optical power on the epidermal face of the tissue was measured by moving a single small-area ( $\sim 0.01 \text{ mm}^2$ ) photodiode over the tissue surface (1 mm separation between photodiode and tissue surface). A narrow-band communications emitter in a TO-46 can (Advanced Optical Components HFE 4093-342 – a communications grade vertical cavity surface emitting laser, VCSEL) was used to transmit light through the skin. It was placed in direct contact with the skin's hypodermal surface. The output power of the emitter was adjusted to ensure that the detector was operating in its linear region for all measurements (i.e. below saturation). The position of the photodiode was manipulated using a computer controlled x-y plotter in conjunction with a data acquisition system. A measurement of transmitted optical power was performed at each of a grid of points on the surface of each skin sample (with a grid resolution of 0.6 – 1.2 mm depending on the thickness of the sample). Each measured

power distribution was made relative to the total transmitted power (as measured empirically using the same setup) and divided by the active area of the photodiode. This resulted in a discrete, empirical representation of the relative power flux distribution for each tissue sample. These measurements were recorded with a DC emitter output, but also apply for higher frequencies relevant to data transfer because of the rapid transport of light through tissue. All measurements were performed within 24 hours post-mortem.

### 3) *Data Analysis*

Regression models were fit to each of the variables measured for the power distributions: the empirically measured total transmittance for each sample,  $T_{tot}$ , and the empirically measured full width at half of the maximum,  $FWHM$ , for each sample. These regression models allow for the estimation of these variables for values of tissue thickness that were not measured experimentally. For the  $T_{tot}$  data, a two parameter exponential model of the form,

$$Y = a_1 * a_2^\ell + \varepsilon$$

was fit to the data [18],[19]. The parameter  $\varepsilon$  represents random error due to population and experimental variation.

For the  $FWHM$  data, a quadratic random coefficient model of the form,

$$Y = a_1 + a_2\ell + a_3\ell^2 + \varepsilon$$

was fit to the data, demonstrating a parametric relationship between  $FWHM$  (variable Y) and the thickness,  $\ell$ , of the sample [18],[19]. As above, the parameter  $\varepsilon$  represents random error due to population and experimental variation. Likelihood ratio tests, LRT, were used to establish the minimum order and number of error terms needed for accurate representation of the data [20].

A least-squares Gaussian model was fit to the power flux distribution of each sample, providing a convenient approximation of the distribution shape. This fit allows these distributions to be simulated for any thickness of interest simply and without using complex photon propagation models such as Monte-Carlo simulation techniques [21]-[22]. The recreation of these distributions is necessary for the analysis of the optical interface design parameters, described in greater detail in the Optical Interface section of this paper. The Gaussian model was of the form,

$$J_{rx\lambda}(r, \theta) = \frac{A}{\sigma\sqrt{2\pi}} e^{-r^2/(2\sigma^2)}$$

and was fit to each of the experimentally measured power distributions. Only one spatial dimension,  $r$ , is considered since the distributions are radially symmetric for all angles,  $\theta$ . Using the same model fitting procedure described above for the  $T_{tot}$  and  $FWHM$  data, an exponential and quadratic random coefficient model were selected to represent the Gaussian model parameters  $A$  and  $\sigma$ , respectively. The curves fit to this data allow for the recreation of any optical power distribution for a desired thickness.

#### *D. Optical Interface Theory*

A generic optical telemetry link can be represented as having three essential components: a transmitter, a receiver and an optical interface. The optical interface, as defined here, consists of the emitter, the transmission medium, the optics and the receiving photodiode. A transcutaneous optical telemetry link, TOTL, is very similar to a fiber optic or free-air optical telemetry link; the only essential difference being the nature of the optical interface. For a TOTL, the transmission medium is biological tissue instead

of an optical fiber or air. The fundamental telemetry link design parameters (the emitter power, the skin thickness, the misalignment of the transmitter and receiver, and the area over which the optics integrate the transmitted light) all interact through the optical interface design, and the tradeoffs between them are made clear by an understanding of this interface. Knowledge of these tradeoffs allows for the design of an optical interface that is optimized for the requirements of the system of which it is a part.

The design of the optical interface (the emitter, photodiode, optics and tissue selection) can be approached as achieving a signal-to-noise ratio that is sufficient for adequate link operation. The receiver hardware being used will dictate the SNR required. For example, commercial optical receivers will often list the minimum signal photocurrent needed for low bit-error rate operation at a given data rate (assuming receiver noise is the dominant noise source, and that a particular data encoding scheme is used). Custom receivers would likely be designed for a certain input range, and would have to be characterized to determine the signal levels required. The optical interface can be designed to ensure that this SNR is achieved at the receiver input, and the parameters pertaining to its design can be optimized relative to the system level constraints (e.g. minimizing the total amount of power dissipated, allowing for certain implant locations/tissue thicknesses, tolerating a certain amount of lateral transmitter-receiver misalignment or minimizing the size of the external optics used). The parameters that can be manipulated to optimize the design of this interface include the emitter wavelength, the emitter power, the tissue type and thickness, the lens type and the misalignment that the link will be designed to tolerate.

Generically, the signal-to-noise ratio at the input of the receiver,  $SNR_i$ , is defined by,

$$SNR_i = \frac{I_s}{I_N} = \frac{P_s R}{I_{Nelec} + P_{Namb} R} \quad (1)$$

where  $I_s$  (A) and  $I_N$  (A) are the photocurrents resulting from incident signal optical power and the photodiode noise current respectively.  $P_s$  is the received signal optical power (W),  $R$  is the photodiode responsivity (A/W),  $I_{Nelec}$  is the input referred current noise for the receiver and  $P_{Namb}$  (W) is the incident optical power due to interfering light sources (such as ambient light).

The signal power,  $P_s$  is defined by,

$$P_s = \int_{A_T} P_{Tx} J_{Rx\lambda} \eta_\lambda dA \quad (2)$$

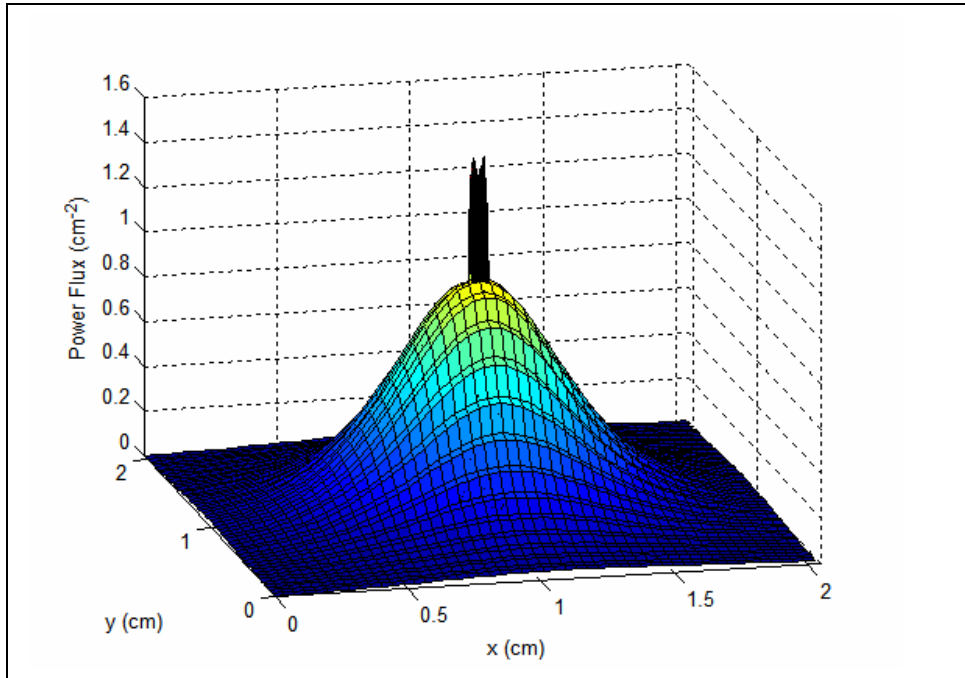
where  $P_{Tx}$  (W) is the optical power of the transmitted pulse,  $J_{Rx\lambda}$  ( $\text{cm}^{-2}$ ) is a function representing the spatial optical power distribution on the receiving surface of the skin at wavelength  $\lambda$ ,  $\eta_\lambda$  is an efficiency factor ( $\eta_\lambda \leq 1$ ) accounting for inefficiencies in optics/optical filters at wavelength  $\lambda$ , and  $A_T$  represents the tissue area over which the receiver optics integrate the signal.

$J_{Rx\lambda}$  is a function of the two spatial dimensions over which the receiving optics integrate the signal light (i.e. the two dimensions of the skin under the receiver), and it represents the flux distribution of exiting photons on the epidermal surface of the skin. For the purpose of discussion, these two dimensions will be referred to as the “interface plane”.  $J_{Rx\lambda}$  is specific to a particular tissue type, and varies with wavelength, tissue thickness, and the optical properties of that tissue. It is this distribution that was empirically measured for the porcine skin samples. One of these distributions (a 4 mm thick sample) can be seen in Figure 1. The optical power flux is made relative to the optical power input by the transmitting emitter.

$A_T$  is the surface under the receiving optics (in the interface plane), over which the transmitted power is integrated by the optics and focused onto the receiving photodiode. The dimensions of  $A_T$  are the dimensions of the area over which the receiver lens integrates the transmitted light (in the interface plane). The exact location of the integration area represented by  $A_T$  is dependent on the axial alignment of the transmitter and receiver: when the transmitter and receiver are perfectly aligned,  $J_{Rx\lambda}$  and  $A_T$  are concentric, and when they are not aligned, the center of  $A_T$  is shifted from that of  $J_{Rx\lambda}$  in the interface plane.

The emitter wavelength,  $\lambda$ , is an important design parameter and should be chosen to maximize power transfer across the skin (minimize absorption and scatter). Skin is an optically turbid media (both scatters and absorbs light) consisting of three layers: the epidermis, the dermis and the hypodermis. The wavelengths in the range of ~800-1300 nm represent a region where photon absorption and scattering are minimal for dermal tissue, creating a region which is optimal for efficient optical power transfer across the skin [16]-[23]. Many commercially available emitters and photodiodes are optimized for operation in this range, as this is the same wavelength range used for many fiber optic and free-air applications. A wavelength of 850 nm was selected for this work because it was within the wavelength region with minimal absorption and scattering, and because the most power efficient commercially available emitters are available at this wavelength.

**Figure 1:** Typical optical power flux distribution,  $J_{Rx\lambda}$  (data for 4 mm sample shown). The surface protruding from the center is the flux distribution of the VCSEL on a 1/500<sup>th</sup> scale.



The efficiency factor  $\eta_\lambda$ , is affected by several factors and can be quite significant. These factors include any transmission inefficiencies in the lens, filter and photodiode window, photons lost due to the acceptance angle of the imaging system and the failure to collect photons with certain paths due to the optics system configuration. Photon loss due to these factors can be quite significant.

The factors that contribute to the input noise current,  $I_N$ , are  $I_{Nelec}$ , the input referred current noise for the receiver and  $P_{Namb}$ , which is the optical power incident on the photodiode that is due to light sources other than the link emitter.  $I_{Nelec}$  is a function of the receiver electronics. The presence, nature and intensity of interfering light sources that contribute to  $P_{Namb}$  can vary greatly depending on environmental conditions. Common interfering light sources include daylight and fluorescent lights.

These various design parameters can all be manipulated to achieve the required SNR<sub>i</sub>; it is the system level design constraints that will dictate the way in which they are configured.

## E. Results

### 1) Transmitted Optical Power Distribution

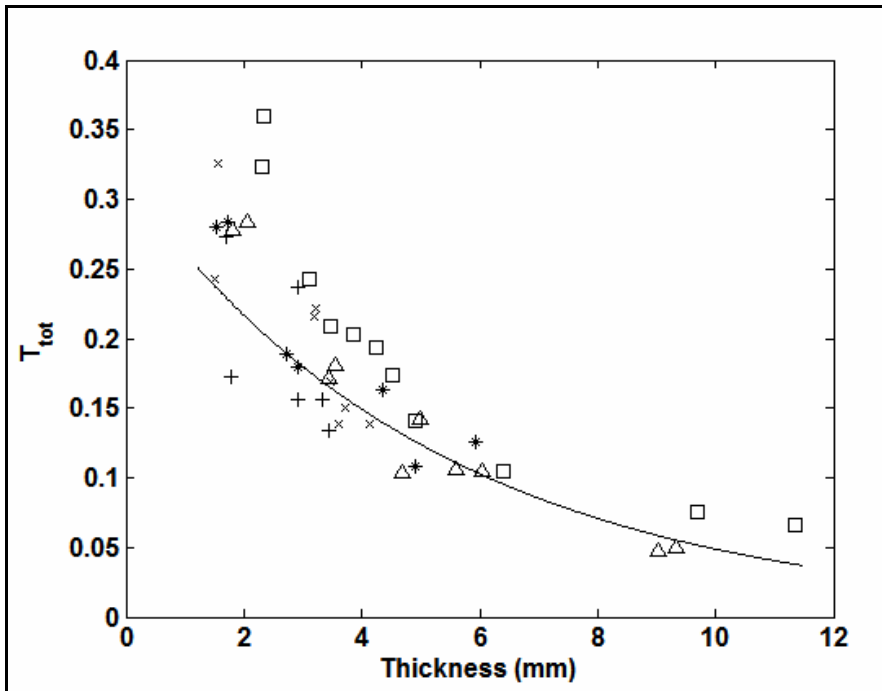
Figure 1 shows a typical optical power flux distribution for a sample that is approximately 4mm thick (normalized to the total input power). The transmitted power is concentrated in the center of the distribution, directly over the emitter. Light that is emitted into the skin is scattered, resulting in a radially symmetric distribution that is spread over the surface of the skin. Overlaid on the same plot in Figure 1 is the power flux from the VCSEL emitter as measured at the TO-46 glass window (Note: the VCSEL distribution is actually plotted on a scale 1/500<sup>th</sup> that of the skin distribution for clarity of

detail). The VCSEL energy is very highly concentrated within a circular area of 0.8mm diameter, and is ring-shaped due to a wire bond in the center of the VCSEL die.

Figure 2 shows the total transmitted fraction of light,  $T_{Tot}$ , for each measured sample (as calculated by numerical integration of the volume under the empirically measured flux distribution) with each sample's thickness. Each marker type in Figure 2 represents samples from one of the five animals in the study. The exponential curve fit allows for the estimation of  $T_{Tot}$  for values of tissue thickness that were not measured experimentally (transmittance estimates for very large thicknesses should be used with caution, as the accuracy of the estimate will decrease with thicknesses beyond the fitted range). Table 1 shows the exponential model fit parameters.

Figure 3 shows the full width at half of the maximum value,  $FWHM$ , for each sample, with each sample's thickness. Each marker type in Figure 3 represents samples from one of the five animals in the study. This plot demonstrates the increasing relative width of the distributions with an increase in thickness. In general, the height of the distributions decreases and the relative width increases with an increase in tissue thickness. This results from an increase in photon absorption and scattering due to the additional hypodermal and adipose tissue present in the thicker samples. LRT showed that a simple quadratic regression model with iid errors was this simplest evaluated model that was sufficient to describe the data ( $p = 1.1e-5$  vs. linear regression with iid errors, and  $p = 0.53$  vs. quadratic random coefficients model with two error sources). As with the previous analysis, this curve fit allows for the estimation of  $FWHM$  for values of tissue thickness that were not measured experimentally (again, estimates for very large

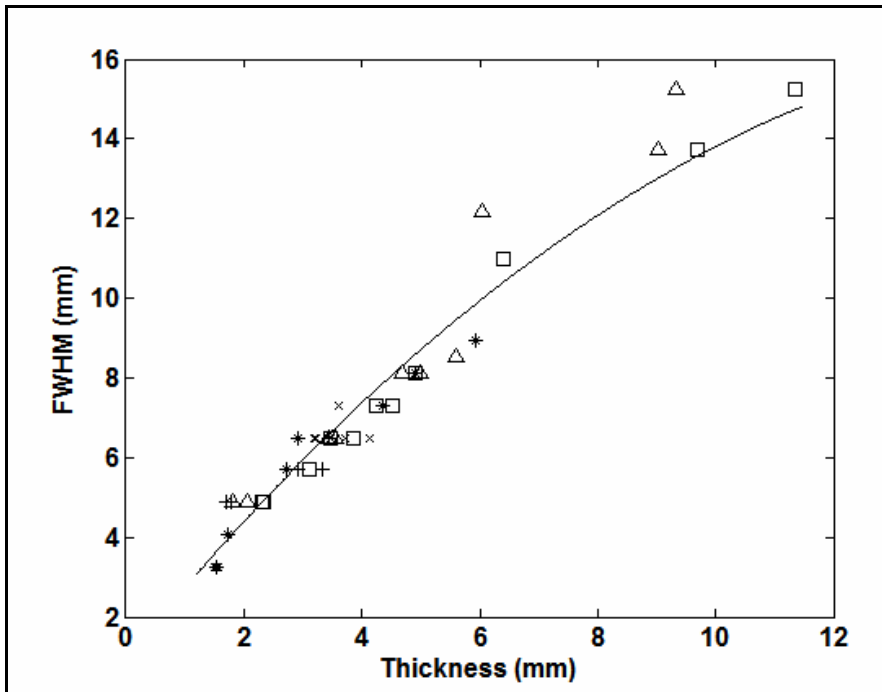
**Figure 2:** Total transmittance with tissue thickness. Each marker type represents samples from one of the five animals in the study.



**Table 1:** Model fit parameters.

$Y$	$a_1$	$a_2$	$a_3$	$\sigma_\varepsilon^2$
$T_{tot}$	0.315	0.830	--	0.00211
$FWHM$	0.991	1.801	-0.052	0.533
$A$	1.808	0.719	--	0.0600
$\sigma$	0.0304	0.0259	-0.00041	0.000055

**Figure 3:** Distribution full width at half maximum with tissue thickness. Each marker type represents samples from one of the five animals in the study.



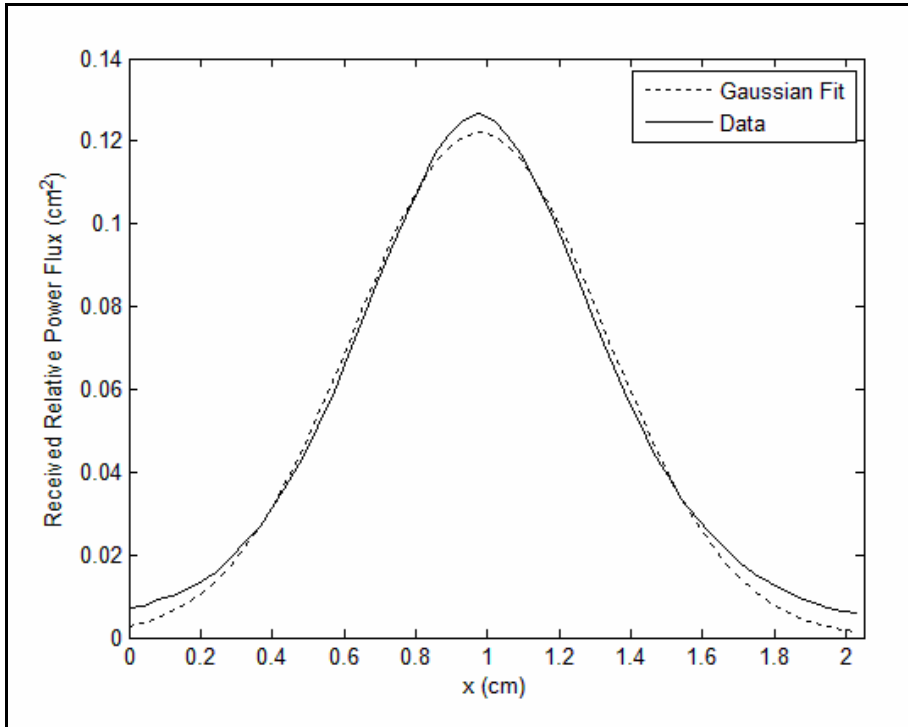
thicknesses should be used with caution). Table 1 shows the parametric model fit parameters.

Figure 4 shows a typical least-squares Gaussian model fit to an experimentally measured distribution for a sample of thickness 3.5 mm. The Gaussian fit provides a sufficient approximation of the distribution shape: the typical mean-squared error is less than 0.5% of the total transmittance, which is well within the variance of the experimentally measured total transmittance. Figure 5 shows the Gaussian model parameters  $A$  and  $\sigma$ , as calculated for each sample, with sample thickness. An exponential and quadratic random coefficient model were selected to represent the Gaussian model parameters  $A$  and  $\sigma$ , respectively. These models allow for the recreation of any optical power distribution for a desired thickness. Table 1 shows the model fit parameters. It is of note that the correlation of  $\sigma$  and  $L$  is 0.987, and that the contribution of the second order coefficient is statistically significant ( $p = 0.0185$ ), but quite small, suggesting that a linear approximation of  $\sigma$  may also be suitable.

## 2) *Optical Interface*

Figures 6 a and b show the optical power flux distribution for light transmitted through two skin samples, with a total thickness of approximately 3 mm and 6.4 mm, respectively. Figures 6 c and d show the data from Figures 6 a and b, but processed to show the total fraction of transmitted optical power that is collected by a perfectly efficient optics system with various lens radii and for various transmitter-receiver misalignments. Each point in Figures 6 c and d was calculated by integrating the distributions shown in Figures 6 a and b, respectively, over a circular region of radius 0

**Figure 4:** Typical Gaussian curve fit to experimentally measured distribution (the data shown is for a sample of thickness 3.5 mm).



**Figure 5:** Gaussian model fit parameters,  $A$  and  $\sigma$ , with sample thickness.

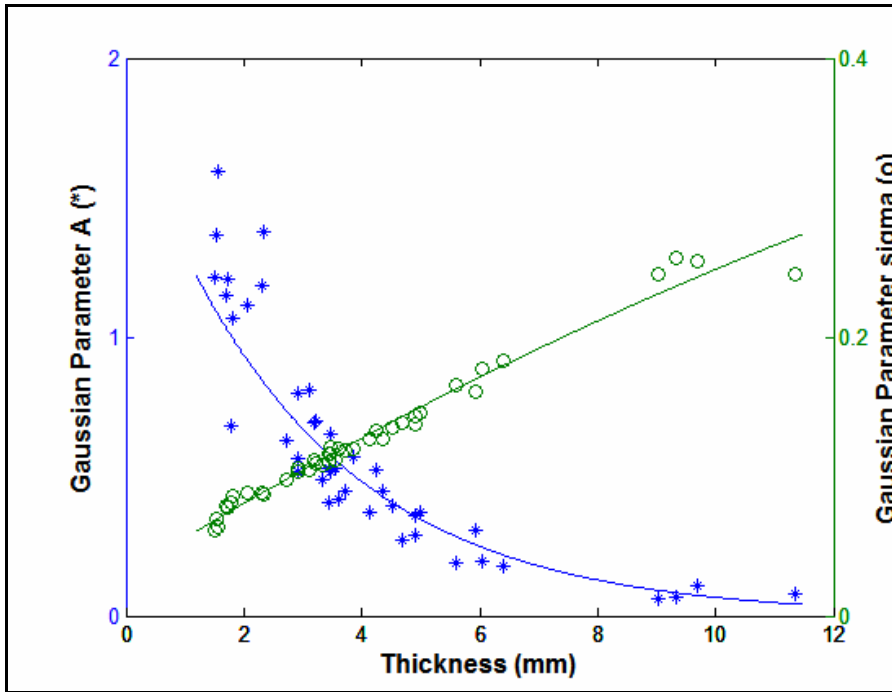
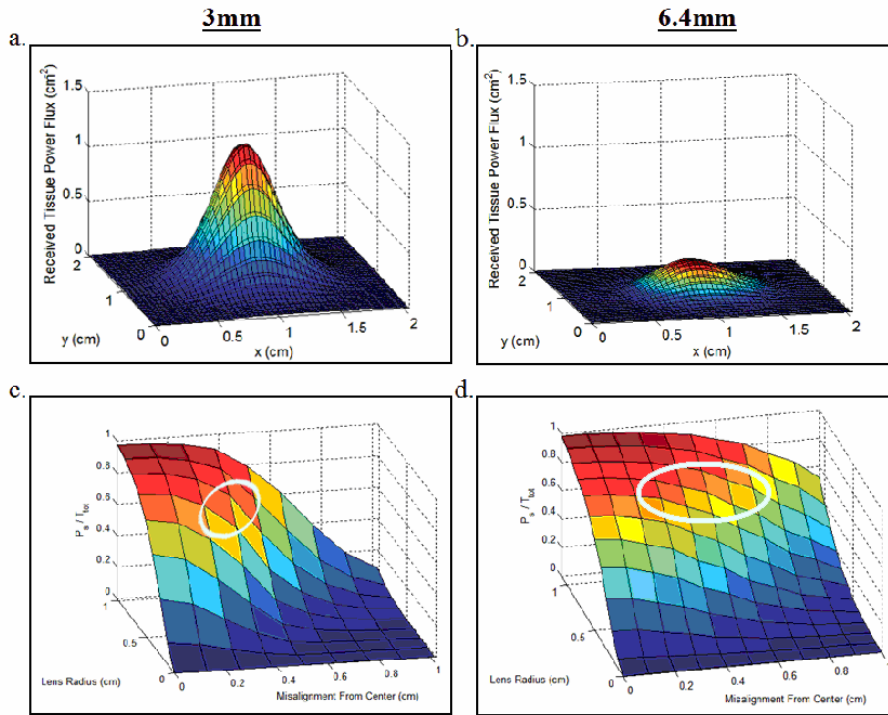


**Figure 6:** a) Power flux distribution for a 3 mm sample, b) Power flux distribution for a 6.4 mm sample, c) Effect of misalignment and lens size on fraction of collected light for a 3 mm sample, d) Effect of misalignment and lens size on fraction of collected light for a 6.4 mm sample.



mm to 11 mm misaligned from the center of the distribution by 0 mm to 10 mm. These plots demonstrate the effect of lens diameter and misalignment on the fraction of total transmitted power collected by the optics system. Since the plots are normalized, it is useful to know the total transmittance for each sample: approximately 0.20 and 0.11 for the 3 mm and 6.4 mm sample, respectively.

These figures show that an increase in lens radius increases the total power collected by the receiver. For each of these two sample thicknesses, a lens radius greater than ~10mm did not result in significant power collection gains. Figures 6 c and d show that an increased transmitter-receiver misalignment results in less total power collected by the receiver. Due to increased scatter and a wider power flux distribution on the epidermal surface of the 6.4 mm sample, Figure 6 d shows a less severe decrease in collected power fraction for a given misalignment than for the 3 mm sample curve.

## *F. Discussion*

### *1) Transmitted Optical Power Distribution*

The  $T_{tot}$  data in Figure 2 clearly shows a significant decreasing trend in the total transmittance with an increase in tissue thickness. Not surprisingly, an increased amount of light-scattering hypodermis and adipose tissue reduces the total amount of power that is transmitted through tissue. This has strong implications for the implant location chosen for the data or power link. For tissue thicknesses of 1.5 mm – 11 mm, the total transmittance ranges from approximately 27% to approximately 5% of the total emitted power. These values are consistent with previously published ranges for  $T_{tot}$  through human skin [24],[25]. This data provides a quantitative means of evaluating the inherent tradeoff between skin thickness and power efficiency. The exponential model fit allows

for the calculation of  $T_{tot}$  for thicknesses that were not measured in this study (although the model will likely misestimate the true transmittance for large thickness values). For example, the total transmittance at a skin thickness of 2 cm is estimated to be approximately 0.0085. Traditional implant locations, such as the abdomen and chest, tend to have fatty deposits of up to several centimeters in thickness, and therefore may be unfavorable for implantation of an optical device because of large power absorption. Choosing an implant location with a very thin dermal covering provides very significant power savings, although the relative power savings per millimeter of tissue diminishes greatly with tissue thickness (e.g. little gain for choosing a site with a dermal thickness of 8 mm over one with a 10 mm thickness, but a large gain when selecting a 3 mm site over a 5 mm site).

Figure 3 demonstrates a near linear relationship between skin thickness and the spread of the power distribution. This has strong implications for the type of optics required for collecting such diffusely distributed light and the effects of receiver-transmitter misalignment. Wider power distributions would require a larger optics integration area to collect sufficient fractions of the transmitted power since it isn't concentrated in a small spatial area. Similarly, the relative amount of light lost by a misaligned transmitter/receiver pair will be less for a wider distribution of light. The parametric model fit to this data allows for the estimation of signal power spread for thicknesses not evaluated in this study.

The Gaussian model provided a reasonably good fit to the flux distributions. This model is a very convenient means of representing these distributions since it only requires two parameters and can be easily recreated using commercial mathematical

analysis software. The reconstruction of a distribution at a given tissue thickness allows one to quantitatively assess the effects of the optics integration area and transmitter-receiver misalignment on the amount of power that is being collected by the receiver. The ability to quantitatively assess the tradeoffs between these design parameters can be quite powerful when designing a transcutaneous data or power link.

## 2) *Optical Interface*

Proper design of the optical interface is integral to achieving a SNR that is sufficient for device operation. The SNR can be maximized by maximizing the signal current and minimizing the noise. With respect to achieving sufficient signal current, Figures 6 c and d quantitatively and powerfully demonstrate the tradeoffs between the various design parameters affecting the optical interface: emitter power, the lens integration area, the misalignment tolerance and the tissue thickness. These plots effectively represent solutions to the equation for  $P_s$  described above (i.e. various operating points for the link). The system level design constraints (implant location requirements, power constraints, misalignment constraints, external device size constraints) will ultimately determine the operating point in this parameter space at which one chooses to operate. For maximizing signal power collection, with all other tradeoffs weighted equally, it is quite evident that there is a region of optimal operation (outlined in white in Figures 6 c and d). These regions are bounded by the minimally accepted misalignment tolerance (~2 mm in Figure 6 for demonstration), and represent the region of maximal signal collection before increases due to larger lens size diminish and significant signal decreases occur due to transmitter-receiver misalignment. It is also evident that while thicker tissue permits less total light to be transmitted, it does provide an advantage in terms of device misalignment tolerance because of the wider power distribution. A larger

lens integration area also results in a greater misalignment tolerance. This analysis could also be relevant to transcutaneous power transfer.

### *G. Conclusions*

We have measured the distribution of optical power flux through porcine skin for skin samples ranging from 2 mm to 11.5 mm in thickness. Two descriptive measures of these distributions,  $T_{tot}$  and  $FWHM$ , were modeled using regression models. Analysis of these measures quantitatively showed the changes in flux distribution shape with tissue thickness. Additionally, the power flux distributions were modeled using a simple, two parameter Gaussian model which allows for the convenient reconstruction of the flux distributions and subsequent analysis of optics collection area and misalignment effects. These distributions were then used to demonstrate the effect that the fundamental optical interface design parameters (lens integration area, misalignment tolerance, emitter power and tissue thickness) have on the amount of power collected by the receiver. This analysis allows for the design of a transcutaneous optical telemetry link that is optimized to certain system-level design constraints: implant location requirements, power constraints, misalignment constraints and external device size constraints.

### *H. Acknowledgements*

This work was supported by NIH-NINDS NS-041809 and NIH-NIBIB EB-001740.

## I. Chapter II Citations

- [1] J. K. Chapin, K.A. Moxon, R.S. Markowitz, M.A.L. Nicolelis “Real-time control of a robot arm using simultaneously recorded neurons in the motor cortex,” *Nature*, vol. 2, no. 7, 1999.
- [2] S. Tillery, D. M. Taylor, R. Issacs, “Online control of a prosthetic arm from motor control signals” *Soc. For Neurosci. Abst.*, vol. 26, 2000.
- [3] M.D. Serruya, N.G. Hatsopoulos, L. Paninski, M.R. Fellows, J.P. Donoghue, “Brain-machine interface: instant neural control of a movement signal,” *Nature*, vol. 416, pp. 141-142, 2002.
- [4] D. M. Taylor, S.I. Tillery, A.B. Schwartz, “Direct Cortical Control of 3-D Neuroprosthetic Devices,” *Science*, vol. 296, no. 5574, pp. 1829-1832, 2002.
- [5] P.H. Peckham, M.W. Keith, K.L. Kilgore, J.H. Grill, K.S. Wuolle, G.B. Thrope, P. Gorman, J. Hobby, M.J. Mulcahey, S. Carroll, V.R. Hentz, A. Wiegner, “Efficacy of an implanted neuroprosthesis for restoring hand grasp in tetraplegia, a multicenter study,” *Arch PM&R*, vol. 82, pp. 1380-1388, October 2001.
- [6] J. Jarvis, S. Salmons, “A family of neuromuscular stimulators with optical transcutaneous control,” *Journal of Medical Engineering and Technology*, vol. 15, no. 2, pp. 53-57, 1991.
- [7] Y. Mitamura, E. Okamoto, M. Tomohisa, “A transcutaneous optical information transmission system for implantable motor-driven artificial hearts,” *ASAIO Transactions*, vol. 36, pp. M278-M280, 1990.
- [8] J.A. Miller, G. Belanger, I. Song, F. Johnson, “Transcutaneous optical telemetry system for an implantable electrical ventricular heart assist device,” *Med. & Biol. Eng. & Comput.*, vol. 30, pp. 370-372, 1992.
- [9] K.I. Inoue, et al., “Transcutaneous optical telemetry system using laser diode,” *Japanese Journal of Artificial Organs*, vol. 27, no. 2, pp. 363-367, 1998.
- [10] M. Sawan, K. Arabi, B. Provost, “Implantable volume monitor and miniaturized stimulator dedicated to bladder control,” *Artificial Organs*, vol. 21, no. 3, pp. 219-222, 1997.
- [11] N. Kudo, K. Shimizu, G. Matsumoto, “Fundamental study on transcutaneous biotelemetry using diffused light,” *Frontiers Med. Biol. Eng.*, vol. 1, no. 1, pp. 19-28, 1988.

- [12] K. Goto, T. Nakagawa, "Transcutaneous photocoupler for transmission of biological signals," *Optics Letters*, vol. 27, no. 20, pp. 1797-1799, 2002.
- [13] B.C. Larson, "An optical telemetry system for wireless transmission of biomedical signals across the skin," Ph.D. dissertation, Dept. Elect. Eng., Massachusetts Institute of Technology, Cambridge, MA, 1999.
- [14] J.L. Abita, W. Schneider, "Transdermal optical communications," *Johns Hopkins APL Technical Digest*, vol. 25, no. 3, pp. 261-268, 2004.
- [15] K.S. Guillory, A.K. Misener, A. Pungor, "Hybrid rf/ir transcutaneous telemetry for power and high-bandwidth data," in *2004 Proc. IEEE Engineering in Medicine and Biology Conf.*, pp. 4338-4340, 2004.
- [16] C. R. Simpson, M. Kohl, "Near-infrared optical properties of ex vivo human skin and subcutaneous tissues measured using the Monte Carlo inversion technique," *Phys. Med. Biol.*, vol. 43, pp. 2465-2478, 1998.
- [17] Y. Du, X. H. Hu, M. Cariveau, X. Ma, G. W. Kalmus, J. Q. Lu, "Optical properties of porcine skin dermis between 900 nm and 1500 nm," *Phys. Med. Biol.*, vol. 46, pp. 167-181, 2001
- [18] M. Davidian, "Applied longitudinal data analysis," New York, NY, Springer, Chapter 8, 2006.
- [19] C.S. Davis, "Statistical Methods for the Analysis of Repeated Measurements," New York, NY, Springer, Chapter 6, 2002.
- [20] G. Verbeke, G. Molenberghs, "Linear Mixed Models for Longitudinal Data," New York, NY, Springer, Chapter 6-8, 2000.
- [21] L. Wang, S.L. Jacques, L. Zheng, "MCML – Monte Carlo modeling of light transport in multi-layered tissues," *Computer Methods and Programs in Biomedicine*, vol. 47, pp. 131-146, 1995.
- [22] A. Krishnaswamy, G.V.G. Baranoski, "A Biophysically-Based Spectral Model of Light Interaction with Human Skin," *Eurographics*, vol. 23, no. 3, pp. 331-340, 2004.
- [23] T.L. Troy, S.N. Thennadil, "Optical Properties of Human Skin in the Near-Infrared Wavelength Range of 1000 to 2200 nm," *J of Biomedical Optics* vol. 6, no. 2, pp. 167-176, 2001.
- [24] J.D. Hardy, H.T. Hammel, D. Murgatroyd, "Spectral Transmittance and Reflectance of Excised Human Skin," *Journal of Applied Physiology*, vol. 9, no. 2, pp. 257-264, 1956.

[25] I.R. Hastie, P.H. Millard, "The quantification of skin transparency," *British Journal of Dermatology*, vol. 108, pp. 315-320, 1983.

**CHAPTER III: PAPER TWO, A HIGH SPEED TRANSCUTANEOUS  
OPTICAL TELEMETRY LINK**

*Chapter III, In Summary*

In summary, the major findings from the work for Chapter III are:

- The technical design specifications for the link are stated
- Simulations showed that a link bit-error rate of only  $10^{-5}$  provides for near-perfect operation of cortical interfacing spike sorting software. This is therefore determined to be the design specification for the data quality required of the link.
- It was demonstrated that a combination of both optical and signal domain filters provides the best noise immunity for the link receiver.
- A transcutaneous optical link capable of transmitting cortical array data was constructed. The table below compares the technical design specifications and the actual operating parameters for the link. Operating parameters are for the case of 3 mm skin thickness.

	<b>Technical Specification</b>	<b>Actual Operating Parameter</b>
<b>Data Rate</b>	40 Mbps	40 Mbps
<b>Maximum Latency</b>	10 mSec	25 nSec
<b>Power</b>	$\leq 100$ mW	4.3 mW @ emitter
<b>BER</b>	$\leq 10^{-5}$	$10^{-10}$ - $10^{-5}$
<b>External Physical Dimensions</b>	Size of behind-the-ear hearing air	SMD components & T1 PD package ( $\sim 1.5$ cm <sup>2</sup> real estate)
<b>Internal Physical Dimensions</b>	$\leq 31$ mm x 25mm x 6mm	SMD components & TO-46 VCSEL package ( $\sim 1$ cm <sup>2</sup> real estate)
<b>Misalignment Tolerance</b>	+/- 2 mm	+/- 2 mm
<b>Components</b>	Commercial OTS when possible	All Commercial OTS
<b>Safety</b>	Maximum permissible exposure $\leq 450$ mW/cm <sup>2</sup>	Actual exposure of 50 mW/cm <sup>2</sup>

## **A High Speed Transcutaneous Optical Telemetry Link**

Authors (in order of appearance):

Ackermann, Jr., D. Michael<sup>1</sup>

Smith, Brian<sup>1</sup>

Kilgore, Kevin L.<sup>2,1,3</sup>

Peckham, P. Hunter<sup>1,3,2</sup>

Affiliations for each author, as indicated by footnote:

<sup>1</sup> Case Western Reserve University, Cleveland, OH, USA

<sup>2</sup> MetroHealth Medical Center, Cleveland, OH, USA

<sup>3</sup> Louis Stokes Veterans Affairs Medical Center, Cleveland, OH, USA

Mailing Address for all authors:

Cleveland FES Center

Hamann 601

2500 MetroHealth Drive

Cleveland, OH 44109

Corresponding Author:

D. Michael Ackermann

Case Western Reserve University

10900 Euclid Ave.

Wickenden Bldg. #313

Cleveland, OH 44113

Phone: 216-368-2948

Fax: 216-368-4969

\*\*\*\*\*

For submission to:

IEEE Transactions on Biomedical Engineering

## CHAPTER III: A HIGH SPEED TRANSCUTANEOUS OPTICAL TELEMETRY LINK

### *A. Abstract*

This chapter is a stand-alone paper that describes the design of a transcutaneous optical telemetry link that is capable of transmitting the 40 Mbps of data generated by a 100-channel cortical microelectrode recording array. This paper presents the technical design specifications for the link, and includes simulations for defining the bit error rate that is required for such a link that is interfacing with a spike sorting system. The performance of the link was assessed at two different tissue thicknesses, 3 mm and 6.5 mm. At the 3 mm thickness, the device was shown to be operational at 40 Mbps with a sufficient bit error rate, consuming 4.3 mW of emitter power, thus satisfying the design specifications.

### *B. Introduction*

In some neural prosthetic applications there is a need for high bandwidth communication between an implanted device and an external device. For example, recent advances have demonstrated the feasibility of real-time cortical interfacing systems [1]-[4]. These systems utilize multiple parallel recordings from microelectrodes or microwires placed in the cortex, and are being developed as a prosthetic control source for the mobility impaired. Because of the limited processing capabilities of current implantable systems and the early stage, developing nature of cortical interfacing, these recorded signals must be transmitted from the implanted device to a processing unit external to the body to be processed into a control signal. Transmitting many channels of

neural waveform data across the skin requires a large communication channel bandwidth. Data rates as high as 40 Mbps may be required for a 100 channel electrode array (assuming a sampling rate of 30 kSamples/sec/channel, 10 bit resolution/sample, 25% modulation/protocol overhead). Other applications may also require high rate transcutaneous data transfer, including peripheral and cranial nerve recording systems, cochlear implants, visual prosthetics and cortical stimulation sensory prosthetics. This paper describes the design of a telemetry link capable of transmitting data at 40 Mbps through skin, a rate which is sufficient for the transmission of 100 channels of neural data.

Transcutaneous data transmission can be achieved via several modalities, including the use of percutaneous wires, acoustic energy and electromagnetic energy (both RF and optical). Each of these modalities was evaluated for its practicality in achieving the BW and SNR required for 40 Mbps data transmission. Cosmesis and the engineering practicality of implementing each method was also evaluated.

While percutaneous wires have been shown to have low rates of infection and failure [5], they are not considered a permanent long-term solution to the need for transcutaneous data transfer due to device cosmesis and patient acceptance. An ultrasonic acoustic link has been used as a means of telemetry for cochlear implants [6] and offers a large potential channel bandwidth, but the modality is poorly documented in literature and utilizes piezoelectric materials which may not be ideal for an implanted device, because of high driving voltages.

Radio (RF) telemetry (inductive and antenna coupled) is a mature, well established technology and has been used for diverse applications, including neuromuscular

stimulators [7], commercial implantable cardioverter defibrillators and commercial cochlear implants for many years. Neural microelectrode recording systems with integrated RF telemetry systems are also being developed [8]-[10]. The primary advantage of RF telemetry systems over other methods of telemetry is the potential transmitter-receiver separation achievable by some of these systems, a distinct advantage with respect to device cosmetics. Current transcutaneous systems have been shown to be capable of data rates of up to several Mbps [8]. Unfortunately, RF telemetry has a major disadvantage with respect to achieving a sufficient BW: radio bandwidth is highly regulated by the Federal Communications Commission (FCC). Frequency bands that can legally be utilized by a medical telemetry device are limited to the Medical Implants Communication Service (MICS) band (402-405 MHz) and the Industrial, Scientific and Medical bands (ISM) [12]. Of the available frequency bands, only a few are realistic candidates for high data rate transcutaneous communication: 902 – 928 MHz, 2.4 – 2.5 GHz and 5.725 – 5.875 GHz. These frequency bands are becoming increasingly crowded because of commonly used wireless communication protocols such as 802.11, Bluetooth and others. Devices operating outside of the MICS or ISM bands must operate at very low power levels, making them more susceptible to interference from other sources. RF telemetry also has two major disadvantages with respect to achieving a sufficient SNR: RF links can have high power requirements and are susceptible to interference from other RF emitters, such as wireless networks, telephones, etc. This may be exacerbated by tissue absorption of RF radiation, which can become quite significant at these higher frequencies, making achievement of required signal strength more difficult than at lower frequencies [13].

Optical telemetry is also a mature, well established technology: fiber-optic and free-air optical communication systems are common in consumer goods and are quite well understood. Optical telemetry offers two significant advantages that make it quite attractive for high rate biotelemetry: the optical portion of the EM spectrum is unregulated worldwide for communications purposes, and interference from other sources is minor, and as shown in this paper, can be reduced through filtering. Since the optical spectrum is unregulated, the bandwidth for a transcutaneous optical telemetry link, TOTL, is limited only by the bandwidth of the transmitting and receiving electronics, and the scattering effects of the skin. Preliminary photon spread data published by Eigensee, et. al. [14], suggests the scattering effects of the skin on bandwidth are negligible at the data rates of interest, and should allow for data rates as high as 100s of Gbps before multipath distortion begins to significantly affect data transmission [15]. Additionally, data is modulated using Intensity Modulation with Direct Detection, IM/DD, where the intensity of the optical field is converted directly into a photocurrent that is proportional to the field power [16],[17]. This allows for simple modulation and demodulation with straightforward circuitry. Optical telemetry has been used for several transcutaneous communication applications. Low to moderate data rate (9.6 kbps – 1 Mbps) implementations include systems for providing command signals or low rate data to or from neuromuscular stimulators [18], artificial hearts or implanted cardiac assist devices [19]-[21], bladder stimulators [22], laboratory animal monitoring systems [23], neural recording systems [24],[25] and generic communication systems [26]. A higher rate implementation has also been developed, showing the feasibility of high rate optical transcutaneous data transfer at rates of 10-80 Mbps [27].

This high rate system required relatively large amounts of power to perform successfully (30-40 mW emitter consumption at 40 Mbps [27]), which would limit the applicability of an optical link for an implanted system. Given the inherent advantages with respect to bandwidth and noise immunity, optical telemetry was deemed the most suitable of the evaluated modalities for high speed transcutaneous data transmission. We designed the telemetry link using the optical interface optimization techniques presented in [Chapter 2], and report that low power, high speed transcutaneous optical telemetry is possible (4.3 mW emitter consumption at 40 Mbps).

The specifications for a TOTL will depend on the application and constraints placed on it by the overall system design. For the link described here, the following design criteria were specified: the required data rate for the TOTL is 40 Mbps. The total transmission latency was specified to be less than 10 ms, assuming the link can consume up to 25% of the total latency allowed (40 ms for updating a 25 Hz stimulus pulse train). The TOTL was specified to be tolerant to a +/- 2 mm lateral transmitter-receiver misalignment (accounting for a patient's aid placing the external hardware). The implant location was specified to be a cavity in the region of the mastoid process of the temporal bone, a common site for the implantation of cochlear implants. This region has a skin covering that is approximately 3-5 mm thick on average [28]. The external receiver, which is planned to be located behind the ear, must be of a size that is similar to that of a behind-the-ear hearing aid. Additionally the device must adhere to nationally accepted safety standards for skin irradiation.

To specify the data transmission quality that was required of the link, simulated transmission errors were imposed on a real cortical microwire recording to determine the

effect of bit error rate on spike recognition. A bit error rate of  $10^{-5}$  errors/bit was found to be sufficient for near-perfect spike detection, and was thus defined to be the minimum design specification for the telemetry link. We believe the identification of this specification to be an important finding, as it allows the design of a link that is as power efficient as possible (the link that is described in this work is capable of operating at very low bit error rates,  $< 10^{-14}$ , but at the expense of emitter power).

### *C. Architecture*

A generic optical telemetry link can be represented as having three essential components: a transmitter, a receiver and an optical interface. The optical interface, as described in [Chapter 2], consists of the emitter, the transmission medium, the optics and the receiving photodiode. A simplified schematic of the device architecture is shown Figure 1.

#### *1) Transmitter*

The transmitter consists of the emitter driver and the emitter. The emitter driver chosen for this work is the Maxim MAX3905 VCSEL driver. This device was chosen because of its appropriate operating range and ease of use. The emitter used in this device is an 850 nm communications VCSEL (Advanced Optical Components HFE 4093-342), chosen for its very high electrical-optical power efficiency.

#### *2) Receiver*

The receiver for this link is a simple two stage device utilizing commercial, off-the-shelf components. The first stage is a high bandwidth transimpedance amplifier, Analog Devices AD8015, with a differential transimpedance of 20 k $\Omega$ . The photodiode used in this work is a Photonic Detectors PDB-C134F, chosen because of its adequate bandwidth,

relatively high responsivity at 850 nm (0.65 A/W), integrated optical filter and relatively large area (1.55 mm<sup>2</sup>). It is operating in photoconductive mode, and is reverse-biased with 1.7 V. The differential output of the TIA is high-pass filtered at 3.2 kHz for noise reduction and drives a high speed comparator, Analog Devices AD8561, for conversion to a logic level.  $V_{tune}$  in Figure 1 places the AC coupled TIA output in an appropriate range for the comparator.

### 3) *Optical Interface*

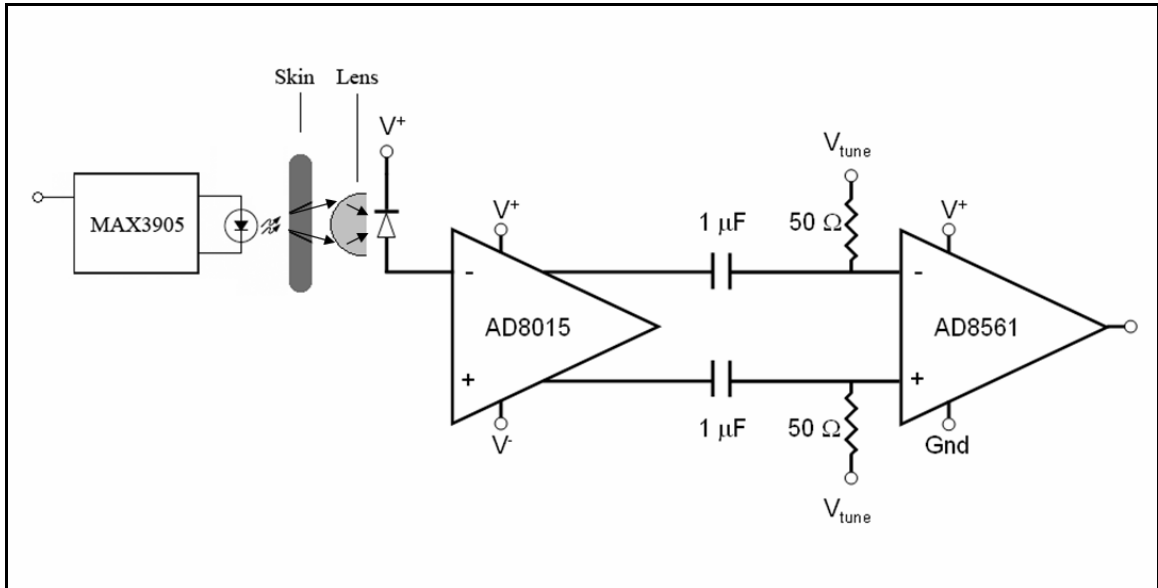
As described in [Chapter 2], the design of the optical interface (i.e. the emitter, photodiode, optics and tissue selection) is quite important. The factors that are controlled as part of the optical interface design include the emitter wavelength, the tissue type and thickness, the lens type and the misalignment that the link is designed to tolerate. For a link operating at 40 Mbps, the following optical interface parameters were chosen: an emitter wavelength of 850 nm, a total tissue thickness of approximately 3 mm (actually 2.8 mm – 2.9 mm thick) and 6.5 mm (two operating points were tested for tissue thickness to simulate implantation of the device in a mastoid cavity, and in a thoracic location), a photodiode-integrated lens (30° viewing angle) with a viewing radius of 1.5 mm, and a misalignment tolerance of +/- 2 mm.

## D. *Methods*

### 1) *Simulation of Transmission Errors*

To determine the quality of transmitted data that is required of a transcutaneous telemetry link, simulated transmission errors were imposed on a neural unit recording, and the effects on spike detection were evaluated. A 10 second segment of neural activity recorded from a microwire, which is thought to be placed in the primary motor

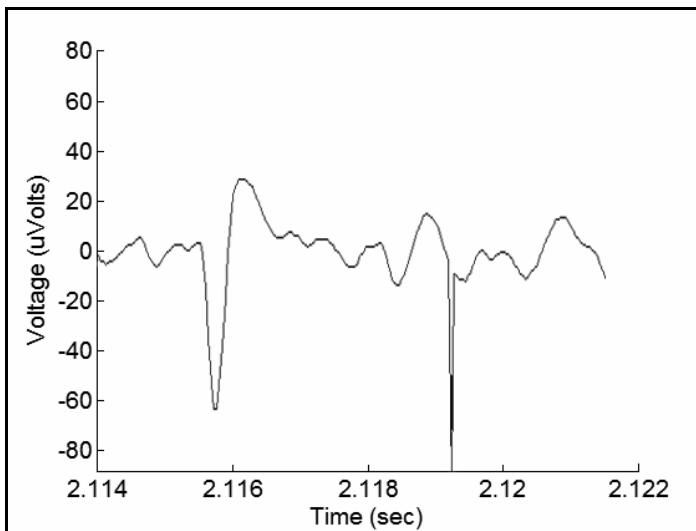
**Figure 1:** Simplified schematic of the transcutaneous optical telemetry link.



cortex of a rhesus macaque monkey was used for evaluation (the neural recording is courtesy of Prof. Dawn Taylor's BCI Laboratory at Case Western Reserve University). The activity was sampled at 24.4kHz, and each sample of the recording had a resolution of 10 bits (the recording was rescaled such that its peak value was 50 % of the dynamic range), resulting in a long string of binary digits ( $2.4 \times 10^6$  bits). The average signal to noise ratio for the recording (ratio of peak-peak spike amplitude to background noise level) was approximately 13.8. Random bit errors were then superimposed on the simulated bit stream, simulating bit errors that are caused by a telemetry link when transmitting data. Since the bit error rate, BER, is the most direct measure of the quality of the data being transmitted through the communication channel, it was used as the independent variable for the simulations. Five different BERs ( $10^{-6}$ ,  $10^{-5}$ ,  $10^{-4}$ ,  $10^{-3}$  and  $10^{-2}$  errors/bit) were evaluated for their effect on spike detection. The bit errors were randomly distributed (uniform distribution) throughout the 10 second bit stream. Each of these bit errors therefore resulted in a change in one of the 10 bits pertaining to a waveform sample. Figure 2 shows a segment of neural data containing a unit spike (at  $t = \sim 2.116$  sec) and a bit error resulting in a false '0' in the second most significant bit of the sample (at  $t = \sim 2.119$  sec).

Two different spike detection methods were evaluated: simple threshold detection (threshold =  $-50 \mu\text{V}$ ), and template matching. These detection methods were selected because they are both methods that can be used for real-time spike detection, and because they represent both a very simple and a moderately complex detection algorithm, respectively [29]. All spike detection was performed using the Cambridge Electronic Design, Inc. Spike2 spike sorting software. Only one template was used for detection for

**Figure 2:** Segment of neural recording containing a spike at  $t = \sim 2.116$  sec and a bit error at  $t = \sim 2.119$  sec.



all of the analyzed waveforms. For each of the five BERs evaluated, five samples containing transmission errors were generated (using the same 10 second recording), and evaluated for spike content.

### 2) *Measurement of Filter Efficacy*

The effects of filtering on the total noise seen by the receiver were measured empirically. Ambient light from a room lit with fluorescent lights, with some sunlight entering through windows, was measured using a high gain TIA with a bandwidth of 400 kHz. The power spectrum of the output (with photodiode pointed at the ceiling) was measured under 4 different conditions: 1. without filters, 2. with an optical filter placed before the photodiode (~750nm to ~1050nm), 3. with the TIA output filtered electrically at 3.2kHz (approximately the highest frequency at which the most significant spectral content was found), 4. with both the optical and electrical filters in place. The power spectrum was integrated from 0.25Hz to 400 kHz to calculate the total noise power.

### 3) *Measurement of Bit Error Rate*

The bit error rate, BER, is the most direct measure of the quality of the data being transmitted through the communication channel and was therefore used to assess performance of the link. For this work, link BER measurements were performed for two different skin samples, one of approximately 3 mm thickness and one of approximately 6.5 mm thickness. These thicknesses were chosen because of their anatomical relevance. A cavity in the mastoid portion of the temporal bone of the skull (the implant location for cochlear implant receivers) and the upper trunk are two candidate implant locations, and these skin samples are loosely representative of skin thicknesses found in these regions (the 6.5 mm sample was the thickest section of skin available for an area with dimensions

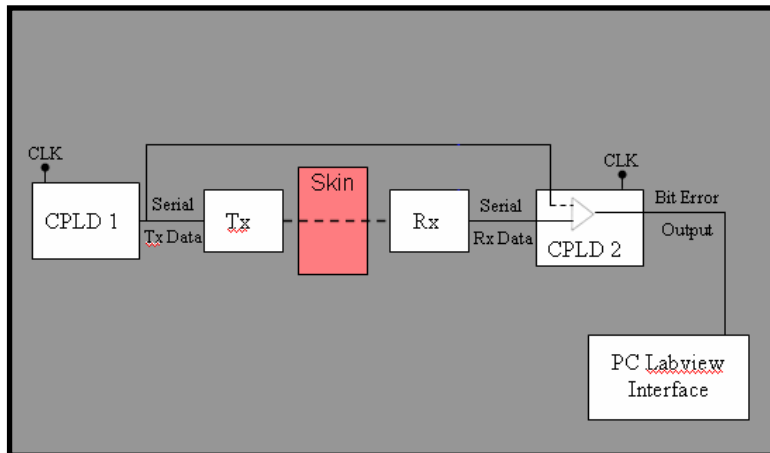
of at least 5cm x 5cm) [28]. The skin was harvested from a Yorkshire-cross farm pig within 5 hours postmortem, and was immediately frozen. Porcine skin was chosen to be a suitable model for human skin because of their similar optical properties [30],[31]. The skin was allowed to thaw to room temperature before link performance was analyzed. For each sample, the BER of the link was measured for varying degrees of lateral transmitter-receiver misalignment, which was manipulated via a computer controlled x-y plotter. BER measurements for each sample were taken for lateral alignment values from well aligned to a 7.0 mm misalignment, in 1.0 mm increments.

As shown in Figure 3, a bit error rate tester was constructed using two Xilinx CoolRunner-II XC2C256 CPLDs and a National Instruments Labview interface. CPLD1 (from Figure 3) generated a continuous  $2^{15}-1$  pseudorandom data stream. The output of the pseudorandom bit sequence generator was XORed with the clock to generate a DC balanced digital waveform (important for a high-pass filtered receiver). This output, the *Tx* data stream, served as input to the emitter driving circuitry of the TOTL. CPLD2 (from Figure 3) received input from both the *Tx* data stream and the output from the TOTL, the *Rx* data stream. CPLD2 compared the two incoming data streams and counted the number of erroneous bits being transmitted. The two CPLDs were synchronously clocked. The *Tx* data stream was delayed 25 ns to account for the delay through the TOTL, and the clock line for CPLD2 was delayed 35 ns to maximize data accuracy when latching. The clock count and erroneous bit count were both output to a Labview interface, which provided the BER information in a GUI.

#### 4) *Lens Viewing Area Optimization*

The lens used for this link is a small diameter, wide acceptance-angle lens that is integrated with the photodiode. This type of lens is not in direct contact with the skin,

**Figure 3:** A simplified diagram showing the experimental setup for testing bit error rate.



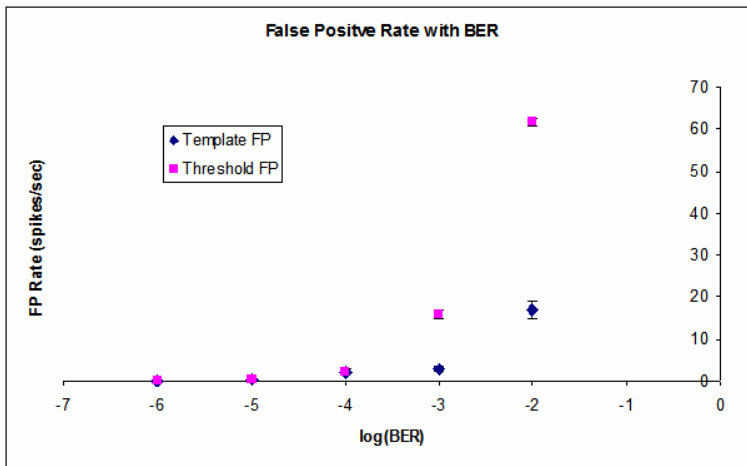
and the optimal separation distance between the lens and the skin must be determined. The circular viewing area for the lens is a function of this separation distance between the photodiode and the top of the skin sample. The lens viewing angle of  $30^\circ$  was used to calculate the radius of the circular portion of the skin viewed by the lens. For a very small viewing radius (resulting from a small lens-tissue separation distance), the lens does not collect much transmitted light because its input is isolated to a small region of tissue. On the other hand, for a very large viewing radius (resulting from a large lens-tissue separation distance), the lens does not collect much transmitted light because very few of the uncollimated photons exiting the tissue ever strike the lens. The same BER experimental setup was used to find the optimal viewing area for the photodiode-integrated lens, by selecting the viewing radius that provided the best BER performance for transmitter-receiver misalignments of 0 to 2 mm.

## *E. Results*

### *1) Simulation of Transmission Errors*

Figure 4 shows the effects of transmission errors on neural spike detection using both threshold and template matching methods. The data is represented as the number of false-positive identified spikes per second. The average measured spike rate for the error-free data (as measured by both the threshold and the template matching algorithms) was 8.3 spikes/sec. This figure shows that there is a significant increase in false-positive spikes with an increase in the BER. Interesting, this data clearly shows that for a BER less than  $10^{-5}$ , there is no significant change in the measured spike rate (which is the output measure for most BCI systems). Error rates for a BER of  $10^{-4}$ , while significant,

**Figure 4:** False positive rate as a function of bit error rate, for both threshold and template matching spike detection.

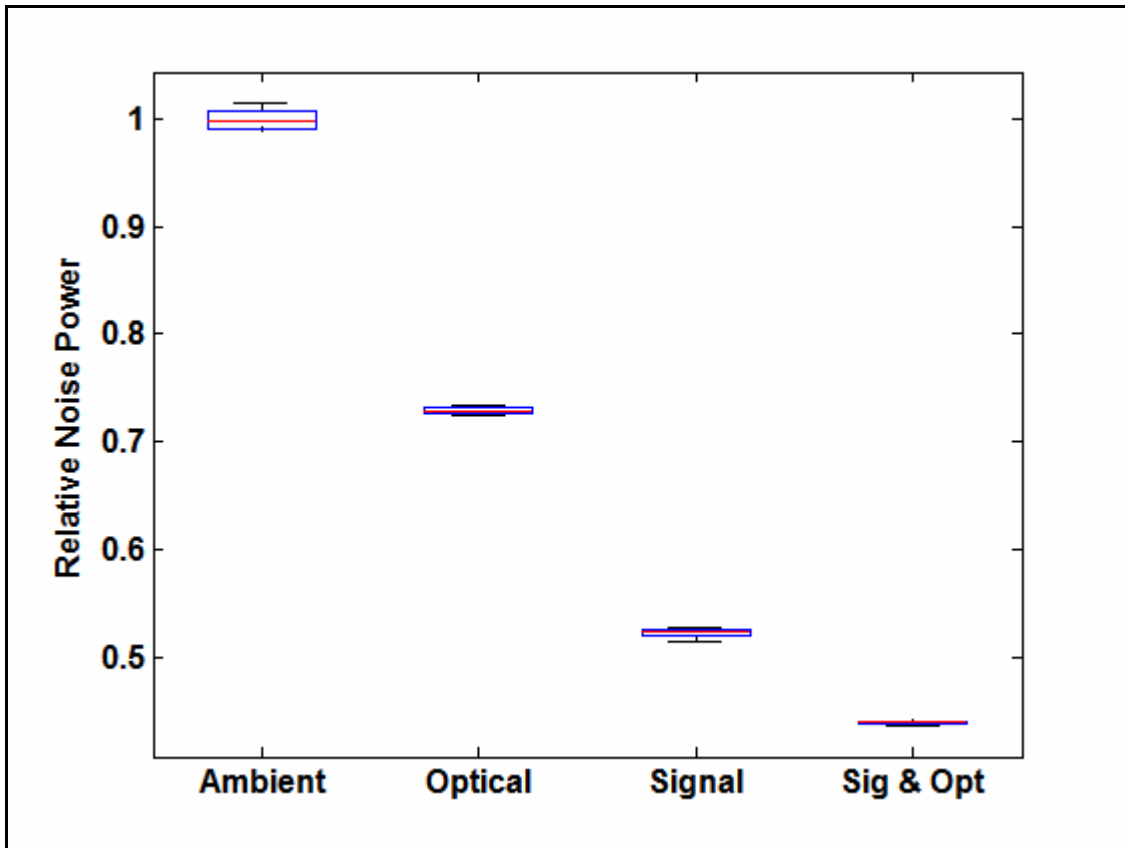


may also be tolerable for some applications (~2 errors/second, or approximately 25% of the actual spike rate for both detection algorithms). While not shown, false negative rates were also computed. This data showed a similar trend to the false-positive data, although there were much fewer erroneous detection decisions (there were zero or fractional spike error rates for BERs of  $10^{-6}$  to  $10^{-3}$ , and three or fewer false-negatives/sec for a BER of  $10^{-2}$ ). The threshold detection algorithm was less tolerant to transmission error than the template matching algorithm, especially for large BER values.

## 2) *Filter Efficacy*

To evaluate the ability of filtering to reduce receiver noise levels, both optical and signal domain filters were applied to a transimpedance amplifier exposed to ambient room light. Figure 5 shows the integration of the photocurrent power spectrum from 0.25 Hz to 400 kHz under the four measured conditions: without filters, with an optical domain filter only, with a signal domain filter only and with both filters applied. These values are normalized to the mean of the case without filters. Each point in Figure 5 represents the average of five measurements. One way ANOVA and Tukey-Kramer multiple comparison tests have shown that each of the conditions was significantly different from each of the others ( $p \ll 10^{-9}$ ). The optical filter alone provided moderate noise reduction of approximately 27% over the measured bandwidth. The high-pass signal domain filter (cutoff of 3.2 kHz) alone provided a greater reduction of approximately 48% over the measured bandwidth. Although it is not evident from Figure 5, the signal domain filter also eliminated the approximately DC (which may drift as ambient conditions change) signal resulting from the ambient light. The combination of both filters resulted in approximately 56% total noise reduction over the measured bandwidth.

**Figure 5:** Effects of the various filters on the relative magnitude of ambient light noise seen by the receiver.



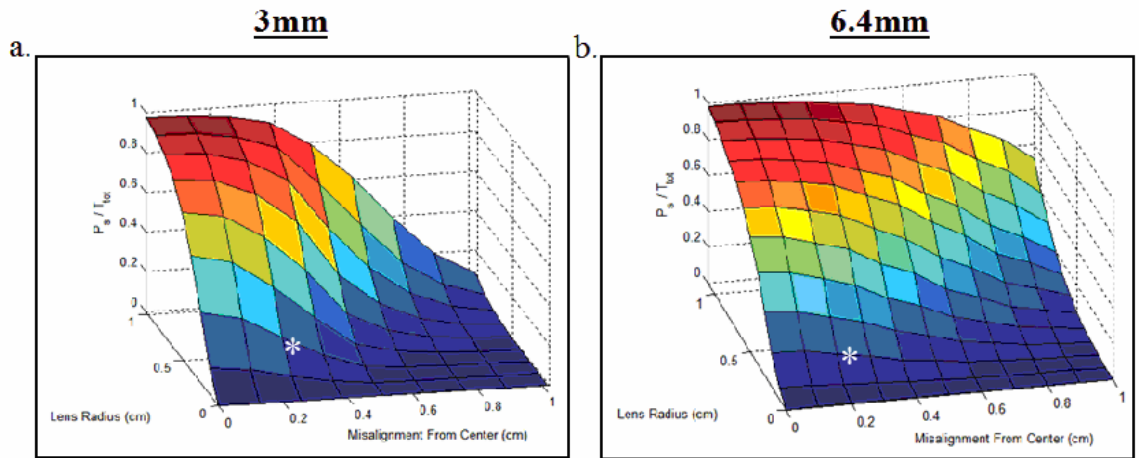
### 3) *Optical Interface*

Figures 6 a and b, as reprinted from [Chapter 2] show the total fraction of transmitted optical power that is transmitted through two skin samples, with a total thickness of approximately 3 mm and 6.4 mm, respectively. The plots represent the fraction of light that is collected by a perfectly efficient optics system with various lens radii and for various transmitter-receiver misalignments [Chapter 2]. The plots are normalized, and the total transmittance for each sample is approximately 0.20 and 0.11 for the 3 mm and 6.4 mm sample, respectively [Chapter 2]. The operating point of the link for each of the two skin thicknesses is represented by the ‘\*’ mark in the respective plots.

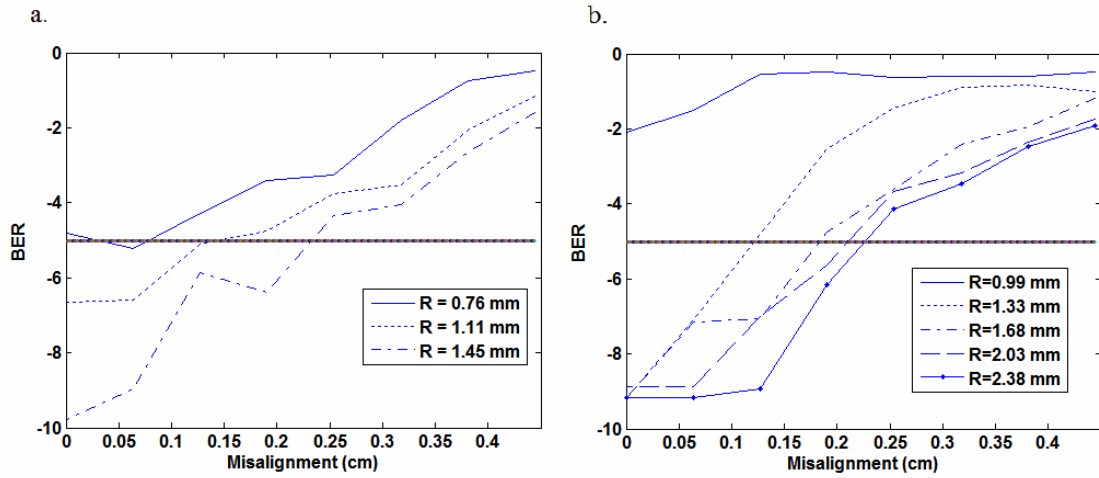
### 4) *Bit Error Rate*

Figure 7a shows the performance of the link transmitting data through the 3mm thick sample, displaying the BER for various degrees of transmitter-receiver misalignment. The three curves represent measurements taken with different lens viewing radii (0.76mm – 1.45mm). For the curves in Figure 7a, the link is operating at 40 Mbps, with an average emitter power of 4.3 mW (calculated as the emitter current multiplied by an emitter voltage drop of 1.7 V). 1.3 mW is dissipated due to the modulation current, which produces optical output (average of 0.76 mA), and the remainder is dissipated due to bias current. This modulation current results in approximately 0.6 mW of emitted optical power (as calculated from the datasheet-specified VCSEL conversion efficiency), with an average duty cycle of 50%. The horizontal black line represents the specified required BER of  $10^{-5}$  errors/bit. With a skin sample thickness of 3 mm, the link is capable of transmitting data at 40 Mbps with a misalignment of +/- 2 mm with a

**Figure 6:** Optical interface operating point for skin thickness of a) 3 mm, and b) 6.4 mm. ‘\*’ marks the operating point. Reprinted from [Chapter 2].



**Figure 7:** BER performance of the link for various transmitter-receiver misalignments and viewing radii for a tissue thickness of a) 3 mm and b) 6.5 mm.



satisfactory BER. Figure 8 shows an eye diagram of the received data when the link is well aligned and transmitting data through the 3 mm skin sample.

Figure 7b shows the performance of the link transmitting data through the 6.5 mm thick sample, displaying the BER for various degrees of transmitter-receiver misalignment. As above, the five curves represent measurements taken with different lens viewing radii (0.99 mm to 2.38 mm). The link is operating at 8 Mbps, a reduction required because of the decrease in power collected by the receiver. The link operated with an average emitter power of 5.1 mW. 2.1 mW is dissipated due to the modulation current (average of 1.2 mA), and the remainder is dissipated due to bias current. This results in approximately 0.96 mW of optical power emitted, with an average duty cycle of 50%. With a skin sample thickness of 6.5 mm, the link is capable of transmitting data at 8 Mbps with a misalignment of +/- 2 mm with a satisfactory BER.

The link was shown to have a total transmission latency of approximately 25 ns.

##### 5) *Lens Viewing Area Optimization*

The optimal viewing area radius for the photodiode-integrated lens is dependent on the sample thickness. This is because of the change in the power distribution on the epidermal surface of the tissue for changes in thickness. Figure 9 shows the effect of the viewing radius on the link BER for transmitter-receiver misalignments of ~0 mm and ~2 mm. The BER decreases with an increase in viewing radius from 0.7 mm to approximately 1.5 mm, because the lens is collecting more light from the increased viewing area. As the viewing area radius increased from 1.5 mm, the lens collected less light, because an increasing fraction of photons have trajectories that do not result in collection by the lens. From this analysis, it is evident that a lens viewing radius of

**Figure 8:** Data eye-diagram for a well aligned link transmitting data through 3 mm skin at 40 Mbps.

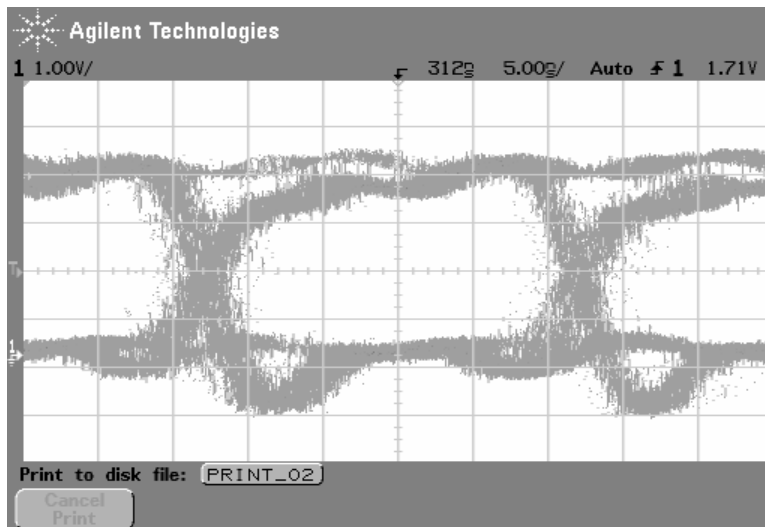
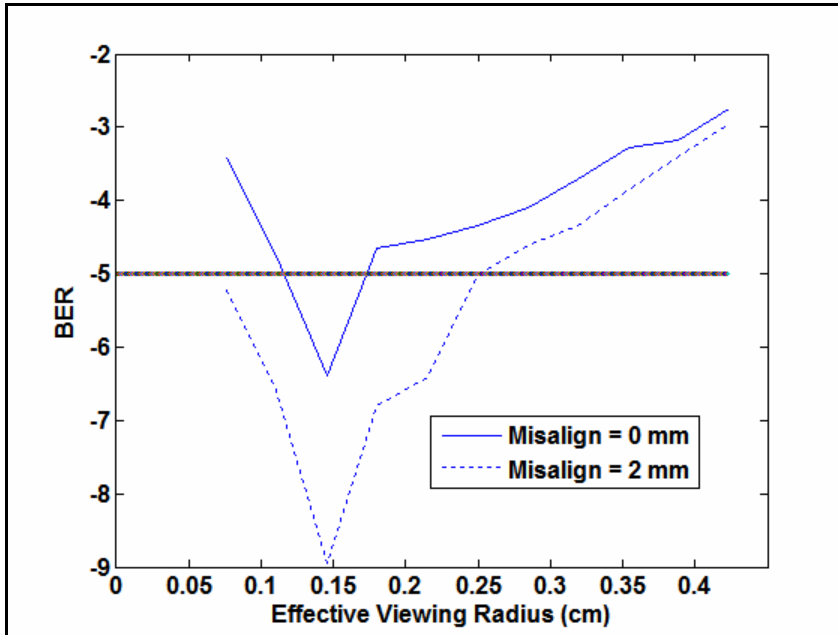


**Figure 9:** Link BER for various lens viewing area radii. Data shown is for transmitter-receiver misalignments of 0 mm and 2 mm.



approximately 1.5 mm is optimal. A similar analysis yields a viewing radius of approximately 2.0 mm for the 6.8 mm sample.

#### *F. Discussion*

The transmission error simulations showed that a link with a BER of  $10^{-5}$  is sufficient for detecting near-perfect spike rates when using both threshold and template matching detection. The identification of this specification allowed the design of a link that is as power efficient as possible. The link described in this work is capable of operating at very low bit error rates ( $< 10^{-14}$ !), but this increase in data accuracy results in a power cost, and does not provide any functional benefit (if the spike rate is the measured variable for the BCI system). Additionally, the low variance of the error rates will also allow for good tolerance of the errors by BCI systems if spike rate change is the measured variable, rather than the spike rate itself.

The TOTL design presented in this work is operating at the point in Figures 6 c and d (for the 3 mm and 6.5 mm implementations, respectively) represented by the ‘\*’ mark, meaning it utilizes a small integration area. While the integration area for the photodiode-integrated lens is small, and the physical separation of the lens and the tissue results in an increased number of photons that do not strike the lens (a low  $\eta_\lambda$ ), it does provide several very significant advantages over other optics configurations. The configuration has an incredibly small profile in all dimensions (T1 package), provides a larger viewing area than the same photodiode without a lens, is quite inexpensive and was shown to collect sufficient signal power for low power operation.

The TOTL utilized hardware developed completely from commercial, off-the-shelf components, which is important for a device that is to be implemented clinically. The

device was shown to be capable of providing transmission of data that would be required by a 100 channel implanted cortical microelectrode array within the specified constraints. The device was shown to operate at a data rate of 40 Mbps, using 4.3 mW of emitter power, with a latency of 25ns, with a BER of  $\leq 10^{-5}$  for a misalignment tolerance of +/- 2mm, given a skin thickness of ~3mm (suitable for implantation in the mastoid cavity). The device operates within ANSI safety standards (a maximum permissible exposure of 450 mW/cm<sup>2</sup> at 850 nm) with a maximum power density ~50 mW/cm<sup>2</sup> [32]. Data transmission through the thicker, 6.5 mm skin sample was also shown to be possible, but required a reduction in the bit rate and an increase in emitter power for the same misalignment and BER performance as the 3 mm sample. This is a result of the decreased transmittance and increased spread of the distribution. The higher efficiency that was achieved with the thinner skin suggests that the mastoid cavity is likely a preferred implant location relative to the chest. In addition to preferable optical properties, the mastoid cavity provides a boney anchor for device stability and could take advantage of surgical techniques utilized for cochlear prosthesis implantation.

Filtering of the received signal is important for reducing the degree of ambient light noise contributing to the SNR. Signal domain filtering at 3.2kHz was shown to greatly reduce noise from ambient light, and optical domain filtering from ~750nm to ~1050nm was shown to reduce noise to a lesser, but also significant degree. The combination of both filters resulted in an even greater reduction. A more narrow-band optical filter would likely provide increased noise rejection. Additionally, proper design of the receiver package can shield the optical interface from ambient light, further reducing receiver noise.

An obvious next step is to develop a device whose optical interface is operating in the region of optimal operation described above. This can be achieved by utilizing an optics system with a larger integration area. Traditional single-lens imaging optics are likely not appropriate for this application, because they require a large separation between the tissue and the photodiode for proper focusing of the power on the photodiode (for relevant integration areas). This results in a low  $\eta_{\lambda}$ , and a very large physical profile (a length of multiples of the integration area diameter). Possible realistic solutions include using a large photodiode with an integrated lens, using fiber optic tapers to converge the light and using multiple photodiodes. A large photodiode with an integrated lens would likely provide the best solution. The factor limiting this configuration is the bandwidth achievable for these photodiodes. Relevant bandwidths can be achieved for photodiodes at least as large as 14 mm in diameter (Hamamatsu S6968), but can require significant reverse bias (10 V+).

A clinical implementation that is implanted in the mastoid cavity could utilize a magnet to ensure proper device alignment, a technique currently utilized by cochlear implant manufacturers. The close proximity of the transmitter and receiver could also provide the opportunity for convenient powering via inductive RF, or optical means. If bidirectional data transfer is required, two different wavelengths could be utilized for full-duplex operation. Additionally, error detection and/or correction would also likely be implemented in a clinical system (line encoding schemes with inherent error detection, such as 8B10B, would likely be preferred). For example, an error detection system could be utilized to notify the user of poor transmitter-receiver alignment.

## *G. Conclusions*

It was found that a bit error rate of  $10^{-5}$  errors/bit is sufficient for near-perfect spike detection, and was thus defined as the design specification for the telemetry link presented in this work. The identification of this specification allowed the design of a link that is as power efficient as possible. The analysis described in [Chapter 2] was utilized to develop a transcutaneous telemetry system capable of transmitting the 40 Mbps of data generated by a 100 channel microelectrode recording array, consuming an average emitter power of 4.3 mW. The consequences of operating with a large skin thickness (less power transfer, and therefore a higher BER or lower bit rate), proposed in [Chapter 2], were demonstrated with a hardware data link.

## *H. Acknowledgements*

The authors would like to thank Dr. Dawn Taylor's BCI lab for the cortical recording data. This work was supported by NIH-NINDS NS-041809 and NIH-NIBIB EB-001740.

### *I. Chapter III Citations*

- [1] J. K. Chapin, K.A. Moxon, R.S. Markowitz, M.A.L. Nicolelis “Real-time control of a robot arm using simultaneously recorded neurons in the motor cortex,” *Nature*, vol. 2, no. 7, 1999.
- [2] S. Tillery, D. M. Taylor, R. Issacs, “Online control of a prosthetic arm from motor control signals” *Soc. For Neurosci. Abst.*, vol. 26, 2000.
- [3] M.D. Serruya, N.G. Hatsopoulos, L. Paninski, M.R. Fellows, J.P. Donoghue, “Brain-machine interface: instant neural control of a movement signal,” *Nature*, vol. 416, pp. 141-142, 2002.
- [4] D. M. Taylor, S.I. Tillery, A.B. Schwartz, “Direct Cortical Control of 3-D Neuroprosthetic Devices,” *Science*, vol. 296, no. 5574, pp. 1829-1832, 2002.
- [5] J.S. Knutson, G.G. Naples, P.H. Peckham, M.W. Keith, “Electrode fracture rates and occurrences of infection and granuloma associated with percutaneous intramuscular electrodes in upper-limb functional electrical stimulation applications,” *Journal of Rehabilitation Research and Development*, vol. 39, no. 6, pp. 671-683, 2002.
- [6] T. Gheewala, R.D. Melen, R.L. White, “A CMOS implantable multielectrode auditory stimulator for the deaf,” *IEEE Journal of Solid-State Circuits*, vol. SC-10, no. 6, pp. 472-479, Dec 1975.
- [7] B. Smith, et al., “An externally powered, multichannel, implantable stimulator-telemeter for control of paralyzed muscle,” *IEEE Trans. Biomed. Eng.*, vol. 45, no. 4, pp. 463-475, Apr 1998.
- [8] M. Ghovanloo, K. Najafi, “A wideband frequency-shift keying wireless link for inductively powered biomedical implants,” *IEEE Transactions on Circuits and Systems-I: Regular Papers*, vol. 51, no. 12, pp. 2374-2383, Dec 2004.
- [9] P. Mohseni, K. Najafi, S.J. Eliades, X. Wang, “Wireless multichannel biopotential recording using an integrated fm telemetry circuit,” *IEEE Trans. Biomed. Eng.*, vol. 13, no. 3, pp. 263-271, 2005.
- [10] N.M. Neihart, R.R. Harrison, “A low-power fm transmitter for use in neural recording applications,” in *2004 Proc. IEEE Engineering in Medicine and Biology Conf.*, pp. 2117-2120, 2004.

- [11] C. E. Shannon, "A Mathematical Theory of Communication," *The Bell System Technical Journal*, vol. 27, pp.379-423, 623-656, Oct 1948.
- [12] Federal Communications Commission, "Code of Federal Regulations, Title 47," 95.601-95.673
- [13] C. Polk, E. Postow, "CRC Handbook of Biological Effects of Electromagnetic Fields," Boca Raton, FL, CRC Press, 1986.
- [14] A. Eigensee, G. Hausler, J. M. Herrmann, M. W. Lindner, "A new method of short-coherence-interferometry in human skin (in vivo) and in solid volume scatterers," *Proc. European Biomedical Optics Week, SPIE 2925*, pp. 169-178, Sept 1996
- [15] J. B. Carruthers, S. Padma, "Estimation of the capacity of multipath infrared channels," *Proc. IASTED Intl. Conf. on Wireless and Optical Communication*, vol. 1, pp.148-153, June 2001.
- [16] S. Alexander, "Optical Communication Receiver Design," USA, SPIE – The International Society for Optical Engineering & The Institution of Electrical Engineers, 1997.
- [17] J. Kahn, J. Barry, "Wireless Infrared Communication," *Proceedings of the IEEE*, vol. 85, no. 2, pp. 265-298, 1997.
- [18] J. Jarvis, S. Salmons, "A family of neuromuscular stimulators with optical transcutaneous control," *Journal of Medical Engineering and Technology*, vol. 15, no. 2, pp. 53-57, 1991.
- [19] Y. Mitamura, E. Okamoto, M. Tomohisa, "A transcutaneous optical information transmission system for implantable motor-driven artificial hearts," *ASAIO Transactions*, vol. 36, pp. M278-M280, 1990.
- [20] J.A. Miller, G. Belanger, I. Song, F. Johnson, "Transcutaneous optical telemetry system for an implantable electrical ventricular heart assist device," *Med. & Biol. Eng. & Comput.*, vol. 30, pp. 370-372, 1992.
- [21] K.I. Inoue, et al., "Transcutaneous optical telemetry system using laser diode," *Japanese Journal of Artificial Organs*, vol. 27, no. 2, pp. 363-367, 1998.
- [22] M. Sawan, K. Arabi, B. Provost, "Implantable volume monitor and miniaturized stimulator dedicated to bladder control," *Artificial Organs*, vol. 21, no. 3, pp. 219-222, 1997.

- [23] N. Kudo, K. Shimizu, G. Matsumoto, "Fundamental study on transcutaneous biotelemetry using diffused light," *Frontiers Med. Biol. Eng.*, vol. 1, no. 1, pp. 19-28, 1988.
- [24] K. Goto, T. Nakagawa, "Transcutaneous photocoupler for transmission of biological signals," *Optics Letters*, vol. 27, no. 20, pp. 1797-1799, 2002.
- [25] B.C. Larson, "An optical telemetry system for wireless transmission of biomedical signals across the skin," Ph.D. dissertation, Dept. Elect. Eng., Massachusetts Institute of Technology, Cambridge, MA, 1999.
- [26] J.L. Abita, W. Schneider, "Transdermal optical communications," *Johns Hopkins APL Technical Digest*, vol. 25, no. 3, pp. 261-268, 2004.
- [27] K.S. Guillory, A.K. Misener, A. Pungor, "Hybrid rf/ir transcutaneous telemetry for power and high-bandwidth data," in *2004 Proc. IEEE Engineering in Medicine and Biology Conf.*, pp. 4338-4340, 2004.
- [28] G. Clark, "Cochlear Implants, Fundamentals & Applications," Springer-Verlag, New York, NY, 2003.
- [29] X. Yang, S.A. Shamma, "A totally automated system for the detection and classification of neural spikes," *IEEE Trans Biomed Eng.*, vol. 25, no. 10, pp. 806-816, Oct. 1988.
- [30] C. R. Simpson, M. Kohl, "Near-infrared optical properties of ex vivo human skin and subcutaneous tissues measured using the Monte Carlo inversion technique," *Phys. Med. Biol.*, vol. 43, pp. 2465-2478, 1998.
- [31] Y. Du, X. H. Hu, M. Cariveau, X. Ma, G. W. Kalmus, J. Q. Lu, "Optical properties of porcine skin dermis between 900 nm and 1500 nm," *Phys. Med. Biol.*, vol. 46, pp. 167-181, 2001
- [32] American National Standards Institute (ANSI), "American National Standard for the Safe Use of Lasers," *ANSI Z136.1*. New York, NY, 2000.

**CHAPTER IV: FUTURE DIRECTIONS FOR IMPLEMENTING A  
TRANSCUTANEOUS OPTICAL TELEMETRY LINK**

## CHAPTER IV: FUTURE DIRECTIONS FOR IMPLEMENTING A TRANSCUTANEOUS OPTICAL TELEMETRY LINK

### *A. Abstract*

This chapter assesses the practicalities of implementing a clinical transcutaneous optical telemetry link. Issues including practical receiver and transmitter design, implant location considerations, device packaging considerations, device powering options and data modulation are considered. Suggestions for successful implementation are also made. It is possible that a TOTL will be implemented with the Networked Neural Prosthesis System being developed by the Cleveland FES Center at Case Western Reserve University. Specific considerations for implementation with this system are considered.

### *B. Implementation with the Networked Neural Prosthesis System*

The Networked Neural Prosthesis System is a sophisticated neural prosthesis platform technology that is currently under development at Case Western Reserve University / Cleveland Functional Electrical Stimulation, FES, Center. The system consists of multiple implanted modules that are connected via a central power and data communication backbone. This battery powered system will be completely implanted for normal device operation and will be scalable to an individual patient's rehabilitation requirements. Like other FES systems, this system will be controlled by a command source modulated by the user (e.g. EMG, volitional movement, etc.).

Complicated control sources, such as large numbers of parallel neural recordings (from the cortex, the spinal cord or peripheral/cranial nerves), will likely not be processed

within the implanted portion of the NNPS due to the complicated control algorithms associated with these signals. These signals will be transmitted across the skin for external processing using a transcutaneous optical telemetry link, TOTL. Figures 1 and 2 show two implementations of such a system, with the transmitter implanted in two different locations, respectively: a surgically prepared cavity in the mastoid portion of the temporal bone of the skull and a subdermal cavity in the thoracic region.

Figure 1 demonstrates how a system with the transmitter implanted in a mastoid cavity might look. The transmitting device would be placed in the excavated cavity in the temporal bone, and the receiver would be worn behind the ear in a device that would look similar to a hearing aid or cochlear implant speech processor. This receiver would be connected to (or integrated with) a digital signal processor that would transform the cortical activity into a control signal. This low data rate control signal would then be transmitted to the implanted portion of the NNPS using a wireless radio link (a link inherent to the NNPS that allows communication with a variety of external devices). As suggested above, the implanted transmitter could also be connected to the NNPS network bus for power and low level command communication.

**Figure 1:** Concept diagram of a TOTL, which is integrated into a cortical recording system. Transmitter is implanted in a mastoid cavity, and transmits data to an external signal processor.

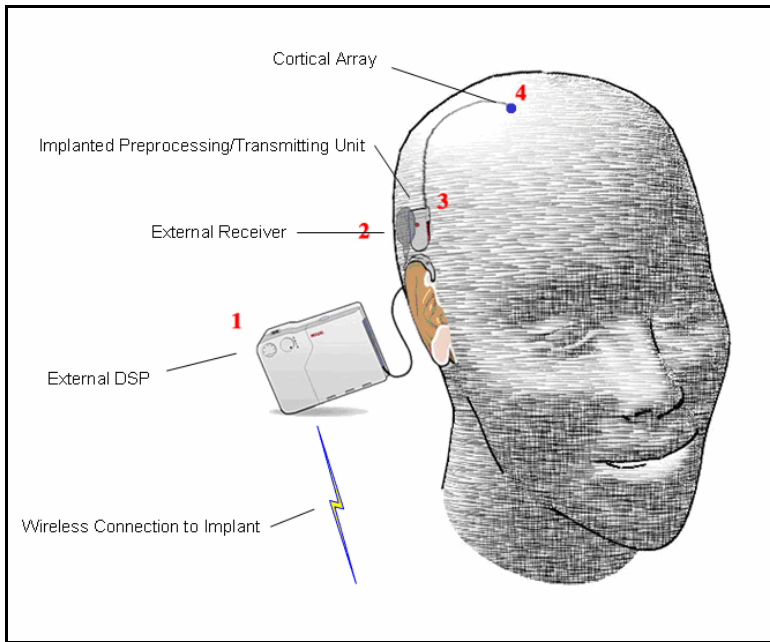


**Figure 2:** Concept diagram of a TOTL, which is integrated into a cortical recording system and the NNPS. Transmitter is implanted in a thoracic cavity, and transmits data to an external signal processor.

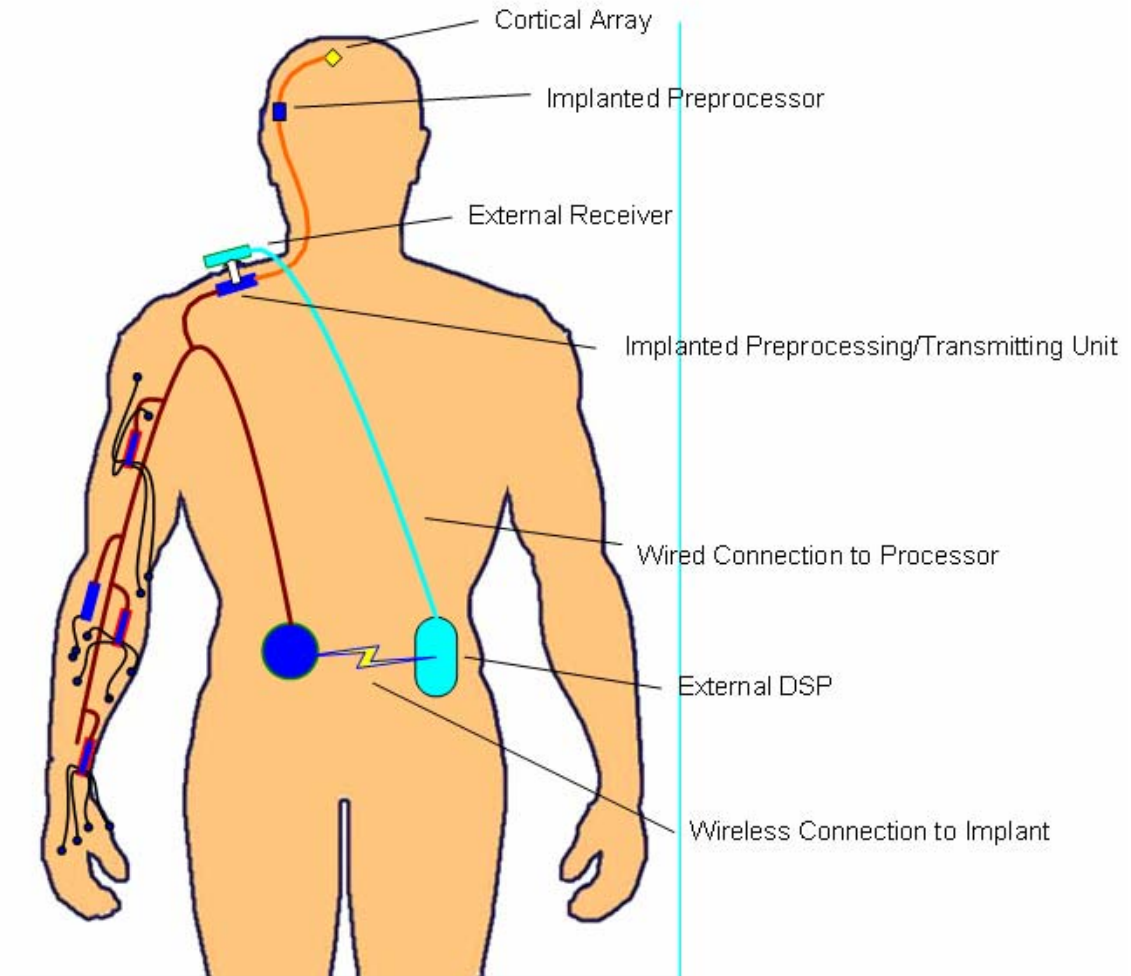


Figure 2 provides an alternate implant configuration, with the transmitter implanted in the thoracic cavity. This configuration is not considered to be optimal. The skin in this region is generally thicker than that covering the mastoid process, the region provides little mechanical stability and the patient would likely have to have an amplification device implanted in the mastoid cavity anyway (to prevent poor SNR, as discussed above). Therefore, the configuration in Figure 1 is recommended for clinical implementation.

### *C. Architecture of a Clinical Transcutaneous Optical Telemetry Link*

The architecture of a clinically realistic implementation will essentially be the same as that described in Chapter 3, but should probably include some hardware improvements and a more sophisticated data handling process. Additionally, such a link will have to take packaging, alignment and other considerations into account. A guideline for implementing a clinically feasible link is provided below.

#### *1) Transmitter Design*

A clinically realistic transmitter would be very similar to, but likely differ slightly from the transmitter described in Chapter 3. Since the transmitter would be implanted, care should be taken to ensure device power consumption is low. The emitter driver circuitry described in Chapter 3 utilized a chip developed by Maxim, Inc. that was intended for use in fiber optic applications, where power is not of paramount concern and data rates of up to 150 Mbps are required (the device quiescent current draw is 14 mA, which is not unrealistic for an implanted system, but is substantial). A reduction in total transmitter power could be achieved by developing minimalist driver circuitry using discrete components. Additional power savings could be possible by reducing the bias

current applied to the VCSEL: a TOTL would be operating at rates significantly lower than the maximum of the operating range for most commercial VCSELs (usually several Gbps), suggesting that operating with a subthreshold bias current may not adversely effect operation.

## 2) *Receiver Design*

The receiver used in a clinical system is less sensitive to power consumption than the transmitter (because it is not an implanted device), and could therefore take one of several different forms. Depending on the requirements of the NNPS, an off-the-shelf single chip solution, or a custom multi-chip solution could be implemented. Several off-the-shelf receiver solutions are available from major semiconductor manufacturers. A clinical system would also require clock recovery circuitry, which was not present in the link presented in Chapter 3. This could be implemented via several methods, including using a discrete phase-locked loop and oscillator, or with an off-the-shelf clock recovery chip solution.

As stated in Chapter 3, a photodiode with an integrated lens would likely provide the optimal compromise of size, optical efficiency and ease of implementation. The data presented in Chapter 2 suggests that a large photodiode (4 to 5 mm diameter) would be the most efficient. Therefore a large photodiode with an integrated lens would be ideal. Photodiodes of this size, with sufficient bandwidth, will likely require a relatively large reverse bias voltage (as large as 10 V). Since the receiver is not an implanted device, this should not be a major problem.

## 3) *Implant Location*

As discussed in Chapters 2 and 3, the location where the transmitter is implanted is quite important. It not only affects system cosmesis and the convenience of operation,

but also affects device operation. A cavity in the mastoid process of the temporal bone is almost certainly the best implant location for such a device, for several reasons. This location would allow for a cosmetically acceptable device, as the external device could be disguised as a behind-the-ear hearing aid, much as cochlear implant transmitters are implemented today. Also, as discussed previously, the skin in this area is quite thin relative to other parts of the body. This has important implications for maintaining low power consumption for the device. This location is also attractive because it would only require established surgical procedures, as this is the same implant location used for cochlear implants. The rigid structure of the temporal bone will provide mechanical stability for the system, which will require intimate alignment of the transmitter and receiver. Additionally, the location is in close proximity to the motor cortex, where the recording array will likely be located. This proximity is important if passive recording electrodes are to be used (i.e. if noise is to be sufficiently low for off-chip amplification).

#### *4) Device Packaging*

The packing for the implanted transmitter will be quite important. Since titanium does not allow for transmission of infrared light waves, a transparent package will be required for transmission of the data. This could be achieved several ways:

- A ceramic package could be used for the entire device, and the transmitter could simply transmit through the package.
- An epoxy, or other transparent packaging material could be used for the entire device, and the transmitter could simply transmit through the package.
- A traditional titanium can could be used for the transmitter circuitry, and a satellite emitter could be used (i.e. feed-throughs would allow access to the emitter, which would be packaged separately from the rest of the circuitry). This is similar to the

concept used by the implantable stimulator-telemeter systems currently used by the Cleveland FES Center, where the inductive coil is located in an epoxy shell peripheral to the titanium stimulator can [14].

5) *Device Powering*

Power for the implanted portion of the telemetry link could be provided by either an external or internal power source. Since the external receiving device will be located within close proximity to the transmitting device, and external power source could conceivably be used. This power transfer could conceivably be provided by inductive, optical or other means. If the link is part of a larger FES system, then power to the transmitter could also be provided internally by the FES system's power source.

6) *Receiver-Transmitter Alignment Stability*

As demonstrated in Chapters 2 and 3, the alignment of the receiver and transmitter is quite important for maintaining receiver SNR. Maintaining this alignment could potentially be achieved using magnets, a method used by some cochlear implant systems. One or more magnets could be located in both the receiving and transmitting devices, allowing the user or patient's aid to simply place the behind-the-ear receiver in close proximity to the transmitter. The magnets would attract each other and ensure that the alignment tolerance is maintained.

7) *Data Modulation*

The way the data is modulated will be quite important for a clinical implementation of a TOTL. A data modulation method known as 8B/10B encoding probably provides the best compromise of bandwidth efficiency, power efficiency, power spectrum

compatibility, clock recovery capability and error detection. This encoding scheme can be implemented with reasonable ease using programmable logic. Low-power complex programmable logic devices, CPLDs, are available commercially. Similar devices are currently being used in the Network Neural Prosthesis System, currently in development at the Cleveland FES Center. Additionally, Xilinx, Inc. and others provide logic cores and development protocols for these devices, making the implementation of an 8B/10B encoder/decoder a reasonable task. 8B/10B encoding also has some inherent error detection capability, adding to its value. For more information on 8B/10B and other encoding schemes, please see Appendix I.

8) *Hardware for the Data Link Layer*

The data link layer (defined by the Open Systems Interconnection, OSI, structure, which is commonly used to define telecommunications systems) consists of the interface that connects the telemetry link to the adjacent device hardware (adjacent device hardware includes the recording array ADC/multiplexer on the transmitting side, and the digital signal processor on the receiving side). This hardware is responsible for encoding and decoding data frames (i.e. addition/removal of header, footer, etc. to the data sequence). The design of the data link layer will be very dependent on the specific requirements of the recording and the control systems with which it is integrated, and will have to be designed with those specific systems in mind. This hardware will be digital in nature, and could be implemented in the same programmable logic devices used for the data modulation.

A simple implementation of this layer could be as follows: The data frame structure could simply be the addition of a one or two byte header (or special 10 bit 8B/10B

character that does't correspond to any 8-bit data sequences, known as 'K characters') to the sequence of the current 100 channel samples, which signal(s) the beginning of the frame [55].

The data link layer also includes error control, which could include error detection and/or correction. True error correction will likely not be necessary. As shown in Chapter 3, spike detection algorithms are quite tolerant to bit errors. 8B/10B encoding has byte-wise error detection inherent to the modulation method. A simple, yet potentially effective strategy could be to watch for these errors, and replace the erroneous bytes with an adjacent value. This strategy would likely reduce some of the erroneous spike detection, particularly for threshold spike detection systems. Additionally, the approximate error rate (as detected by the decoder) could be output to the control processing hardware/software, providing a mechanism by which the user could be notified of a poor connection. Error control is further discussed in Appendix I.

#### *D. Conclusions*

In summary, a transcutaneous optical telemetry link, TOTL, that is capable of transmitting the 40 Mbps of data generated by a 100 channel microelectrode recording array was constructed. Optical telemetry was chosen because of the very large available bandwidth, the lack of interfering sources, and the ease of modulation and demodulation associated with optical telemetry.

To construct this link, an analysis of the transmitter-skin-receiver interface (described herein as the "optical interface") was performed. This analysis demonstrated the tradeoffs between the optical interface design parameters, and allowed for the directed

design of the actual hardware link. This analysis yielded insight into the effect of skin thickness on link design.

This analysis required empirically measured power distributions from porcine skin samples. Specifically, two descriptive measures of these distributions,  $T_{tot}$  and  $FWHM$ , were modeled using regression models. Analysis of these measures quantitatively showed the changes in flux distribution shape with tissue thickness. Additionally, the power flux distributions were modeled using a simple, two parameter Gaussian model, which allows for the convenient reconstruction of the flux distributions and subsequent analysis of optics collection area and misalignment effects.

Two other experiments were performed to facilitate the design of the TOTL. Experiments to determine an optimal combination of filters for the hardware design of the TOTL were performed, showing that the use of both an electrical and an optical filter provided the best receiver noise immunity. Additionally, simulations and a subsequent analysis were performed to determine the BER that is required of a transcutaneous telemetry link used for neural spike data. It was found that a BER of only  $10^{-5}$  is sufficient for near-perfect operation of spike detection algorithms. This analysis helped to dictate the design specifications of the link.

A link similar to the one described in this document may someday be integrated into the Networked Neural Prosthesis System, providing a means for transmitting the large amounts of data generated by cortical microelectrode arrays to an externally located signal processor. This final chapter provides some insight into what is required for implementing a clinically robust TOTL.

## APPENDIX I: DATA MODULATION AND ERROR CONTROL

### *A. Data Modulation*

Before raw data (e.g. the bits that represent the neural data) is transmitted across a telemetry link, it must be encoded in a way that makes it suitable for doing so. The way in which data is encoded (i.e. the ‘line code’ or ‘modulation scheme’) is quite important and can effect the bandwidth and power requirements of the link, among other factors. Many different line codes have been designed, each with varying characteristics. In general, the line code used in any optical communication system (and perhaps for any telemetry system) should have the following attributes: suitable bandwidth efficiency, suitable power efficiency, a power spectrum density that is appropriate for the communication channel (i.e. has a spectrum that is commensurate with the bandwidth of the input and filtering stages), ability to extract the clock from the data stream, is data transparent (i.e. can transmit the data regardless of the number of sequential 1’s or 0’s), some error correction and/or detection capability, and be implemented reasonably in hardware. [56]

There are many commonly used line codes. Some of the more common schemes include on-off keying (non-return-to-zero, NRZ and return-to-zero, RZ), pulse position modulation schemes, subcarrier modulation schemes and run-length-limited schemes. In general, bandwidth is often traded for power efficiency, error correction capability, power spectrum shaping, clock recovery and/or data transparency.

On-off keying, OOK, is one of the simplest modulation techniques and is the simplest to implement. OOK is implemented by simply turning the optical source on or off corresponding to serial binary 1’s or 0’s. There are two general types of OOK, non-

return-to-zero, NRZ, and return-to-zero, RZ. OOK using NRZ pulses utilizes bit pulses that are high or low for the duration of the bit period, where OOK using RZ pulses utilizes high pulses that are only high for a fraction of the bit period. While OOK line codes are simple (direct modulation of the emitter with the data stream), they are very poor choices for data transmission. OOK schemes have a non-zero DC component in the power spectrum, are not transparent to long strings of 1's or 0's (i.e. cannot provide clock information in this case) and do not provide any inherent error correction or detection. [56]

Pulse position modulation, PPM, is slightly more difficult to implement than OOK, but can provide significant increases in power efficiency. This increase in power efficiency also comes at the expense of bandwidth efficiency. PPM is an encoding technique which utilizes serial digital signals consisting of equal length time segments called chips. Only one of  $L$  total chips is high for any given symbol, and digital information is encoded by the position of this high chip. For example, consider a symbol consisting of 4 chips. Two bits of binary data can be encoded in the symbol based on the four possible positions for the high chip (requiring twice the bandwidth for the same data rate) [23]. PPM using  $L$  chips is referred to as  $L$ -PPM. The primary advantage of PPM schemes are their inherent power efficiency (only  $1/L$  chips are high), making them the line code of choice for some standard wireless infrared protocols [57]. Deficiencies of PPM schemes include their bandwidth inefficiency and non-ideal spectral densities. Variations on the  $L$ -PPM code also exist, including differential pulse position modulation, DPPM, and pulse interval modulation, PIM. These codes have similar advantages and deficiencies as  $L$ -PPM [23].

Subcarrier modulation is the modulation of digital binary information onto a carrier wave (modulation of an oscillating light intensity, not of the actual EM waves as with RF telemetry). Subcarrier modulation schemes include some common RF modulation schemes: amplitude shift keying, ASK, frequency shift keying, FSK and phase shift keying, PSK. Subcarrier modulation is not ideal for optical communication since the DC optical offset required for the carrier signal (there is no negative optical power) makes these schemes inherently very power inefficient. [23]

Run-length-limited, RLL, modulation schemes are considerably more complicated than most other modulation schemes, but they can provide incredible advantages. RLL encoding schemes are almost universally used in the fiber optics industry and the high volume data storage industry (hard-drives). RLL codes are different from all of the previously mentioned schemes in that the encoding of one symbol is dependent on the value of the previous symbol and symbols can be of varying length [58].

RLL(d,k) refers to RLL modulation with a run length of d and run limit of k. The run length is the minimum number of chips after a chip transition before another transition takes place. For example, if a RLL scheme dictates a run length of 2, then there will be a minimum of two low chips after a high→low transition and a minimum of two high chips after low→high transition. The run length is frequently only 1 bit, unless receivers with poor frequency response are used. The run limit is the maximum number of chips after a chip transition before another transition takes place. For example, if a RLL scheme dictates a run limit of 7, then there will be a maximum of seven low chips after a high→low transition and a maximum of seven high chips after low→high transition. Having a large run limit allows for more unique chips and can allow greater power

efficiency, but increases the complexity of the encoding scheme and increases the likelihood that the transmitter and receiver will become desynchronized. [58]

8B/10B is a RLL(1,5) code that is very commonly used in the fiber optics industry. The code maps every possible 8 bit combination to a 10 bit equivalent. For this 25% loss in bandwidth efficiency, 8B/10B encoding provides incredible benefit: the code is byte oriented (common to most digital systems), allows for simple clock recovery, has zero DC spectral content and also provides inherent error detection (due to the way the bits are encoded, the code provides 2 inherent means of error detection) [59]. Additionally, since the mapping solution of the 8 input bits to the 10 output bits is non-unique, the power spectrum density of the encoding scheme can be manipulated if the communication channel requires it [56]. For these reasons, 8B/10B encoding is likely the most appropriate for a transcutaneous optical telemetry link.

### *B. Error Control Coding*

If error detection is not sufficient, and error correction is necessary, error control must be employed. Many error control techniques exist and they vary in their control principle, effectiveness and complexity. Most error control techniques can be categorized as redundant control, forward error correction, retransmission control or a combination of the three [57]. Redundant techniques simply have inherent data redundancy, allowing the receiving data processor to make most single errors unimportant [57]. The most complex error control techniques employ the principle of forward error correction [57]. Forward error correction techniques utilize code that enables the receiver to correct erroneous transmitted data without feedback to the transmitter. When bi-directional communication

is possible, retransmission error control can be used. Retransmission control techniques enable the receiver to detect an error and request that the information be transmitted again if necessary. Retransmission control techniques tend to be reliable and are often used when low data error is critical. This reliability comes at the obvious cost of latencies that accompany retransmissions.

Most transcutaneous telemetry systems would likely not require error correction. Chapter 3 describes simulations that examine the effect of transmission errors on spike detection. These simulations suggest that transmission errors are well tolerated by spike detection systems, and that error control is likely not necessary for a link transmitting cortical data. One exception to system tolerance to transmission errors would be a link that was utilized for programming an implant, where data integrity would be paramount. For such a system, an error control paradigm would almost certainly be implemented (likely a retransmission scheme due to its ease of implementation).

## CITATIONS FOR CHAPTERS I AND IV

- [1] J. K. Chapin, K.A. Moxon, R.S. Markowitz, M.A.L. Nicolelis "Real-time control of a robot arm using simultaneously recorded neurons in the motor cortex," *Nature*, vol. 2, no. 7, 1999.
- [2] S. Tillery, D. M. Taylor, R. Issacs, "Online control of a prosthetic arm from motor control signals" *Soc. For Neurosci. Abst.*, vol. 26, 2000.
- [3] M.D. Serruya, N.G. Hatsopoulos, L. Paninski, M.R. Fellows, J.P. Donoghue, "Brain-machine interface: instant neural control of a movement signal," *Nature*, vol. 416, pp. 141-142, 2002.
- [4] D. M. Taylor, S.I. Tillery, A.B. Schwartz, "Direct Cortical Control of 3-D Neuroprosthetic Devices," *Science*, vol. 296, no. 5574, pp. 1829-1832, 2002.
- [5] P.H. Peckham, M.W. Keith, K.L. Kilgore, J.H. Grill, K.S. Wuolle, G.B. Thrope, P. Gorman, J. Hobby, M.J. Mulcahey, S. Carroll, V.R. Hentz, A. Wiegner, "Efficacy of an implanted neuroprosthesis for restoring hand grasp in tetraplegia, a multicenter study," *Arch PM&R*, vol. 82, pp. 1380-1388, October 2001.
- [6] Webster, J. (1998). *Medical Instrumentation, Application and Design*. New York, NY, John Wiley & Sons, Inc.
- [7] Bossetti, C., J. Carmena, et al. (2004). "Transmission Latencies in a Telemetry-Linked Brain-Machine Interface." *IEEE Transactions on Biomedical Engineering* 51(6): 919-924.
- [8] A.X. Widmer, P.A. Franaszek, "A DC-Balanced, Partitioned-Block, 8B/10B Transmission Code", *IBM J. Res. Develop.*, vol. 27(5), 1983.
- [9] C.E. Shannon, "A Mathematical Theory of Communication", *The Bell System Technical Journal*, vol. 27, pp. 379-423, 623-656, 1948.
- [10] H. Nyquist, "Certain Topics in Telegraph Transmission Theory", *AIEE Trans.*, vol. 47, p. 817, 1928.
- [11] J.S. Knutson, G.G. Naples, P.H. Peckham, M.W. Keith, "Electrode fracture rates and occurrences of infection and granuloma associated with percutaneous intramuscular electrodes in upper-limb functional electrical stimulation applications," *Journal of Rehabilitation Research and Development*, vol. 39, no. 6, pp. 671-683, 2002.
- [12] Gheewala, T., R. Melen, et al. (1975). "A CMOS Implantable Multielectrode Auditory Stimulator for the Deaf." *IEEE Journal of Solid-State Circuits* SC-10(6): 472-479.

- [13] Odom, B. (1999). "Ultrasound Analog Electronics Primer." Analog Dialogue 33(5).
- [14] B. Smith, et al., "An externally powered, multichannel, implantable stimulator-telemeter for control of paralyzed muscle," IEEE Trans. Biomed. Eng., vol. 45, no. 4, pp. 463-475, Apr 1998.
- [15] M. Ghovanloo, K. Najafi, "A wideband frequency-shift keying wireless link for inductively powered biomedical implants," IEEE Transactions on Circuits and Systems-I: Regular Papers, vol. 51, no. 12, pp. 2374-2383, Dec 2004.
- [16] P. Mohseni, K. Najafi, S.J. Eliades, X. Wang, "Wireless multichannel biopotential recording using an integrated fm telemetry circuit," IEEE Trans. Biomed. Eng., vol. 13, no. 3, pp. 263-271, 2005.
- [17] N.M. Neihart, R.R. Harrison, "A low-power fm transmitter for use in neural recording applications," in 2004 Proc. IEEE Engineering in Medicine and Biology Conf., pp. 2117-2120, 2004.
- [18] Federal Communications Commission, "Code of Federal Regulations, Title 47," 95.601-95.673.
- [19] C. Polk, E. Postow, "CRC Handbook of Biological Effects of Electromagnetic Fields," Boca Raton, FL, CRC Press, 1986.
- [20] Eigensee, G. Hausler, J. M. Herrmann, M. W. Lindner, "A new method of short-coherence-interferometry in human skin (in vivo) and in solid volume scatterers," Proc. European Biomedical Optics Week, SPIE 2925, pp. 169-178, Sept 1996
- [21] J. B. Carruthers, S. Padma, "Estimation of the capacity of multipath infrared channels," Proc. IASTED Intl. Conf. on Wireless and Optical Communication, vol. 1, pp.148-153, June 2001.
- [22] S. Alexander, "Optical Communication Receiver Design," USA, SPIE – The International Society for Optical Engineering & The Institution of Electrical Engineers, 1997.
- [23] J. Kahn, J. Barry, "Wireless Infrared Communication," Proceedings of the IEEE, vol. 85, no. 2, pp. 265-298, 1997.
- [24] J. Jarvis, S. Salmons, "A family of neuromuscular stimulators with optical transcutaneous control," Journal of Medical Engineering and Technology, vol. 15, no. 2, pp. 53-57, 1991.

- [25] Y. Mitamura, E. Okamoto, M. Tomohisa, "A transcutaneous optical information transmission system for implantable motor-driven artificial hearts," *ASAIO Transactions*, vol. 36, pp. M278-M280, 1990.
- [26] J.A. Miller, G. Belanger, I. Song, F. Johnson, "Transcutaneous optical telemetry system for an implantable electrical ventricular heart assist device," *Med. & Biol. Eng. & Comput.*, vol. 30, pp. 370-372, 1992.
- [27] K.I. Inoue, et al., "Transcutaneous optical telemetry system using laser diode," *Japanese Journal of Artificial Organs*, vol. 27, no. 2, pp. 363-367, 1998.
- [28] M. Sawan, K. Arabi, B. Provost, "Implantable volume monitor and miniaturized stimulator dedicated to bladder control," *Artificial Organs*, vol. 21, no. 3, pp. 219-222, 1997.
- [29] N. Kudo, K. Shimizu, G. Matsumoto, "Fundamental study on transcutaneous biotelemetry using diffused light," *Frontiers Med. Biol. Eng.*, vol. 1, no. 1, pp. 19-28, 1988.
- [30] K. Goto, T. Nakagawa, "Transcutaneous photocoupler for transmission of biological signals," *Optics Letters*, vol. 27, no. 20, pp. 1797-1799, 2002.
- [31] B.C. Larson, "An optical telemetry system for wireless transmission of biomedical signals across the skin," Ph.D. dissertation, Dept. Elect. Eng., Massachusetts Institute of Technology, Cambridge, MA, 1999.
- [32] J.L. Abita, W. Schneider, "Transdermal optical communications," *Johns Hopkins APL Technical Digest*, vol. 25, no. 3, pp. 261-268, 2004.
- [33] K.S. Guillory, A.K. Misener, A. Pungor, "Hybrid rf/ir transcutaneous telemetry for power and high-bandwidth data," in *2004 Proc. IEEE Engineering in Medicine and Biology Conf.*, pp. 4338-4340, 2004.
- [34] International Commission on Non-Ionizing Radiation Protection. "ICNIRP statement on light-emitting diodes (LEDs) and laser diodes: implications for hazard assessment," *Health Physics*, vol. 78, no. 6, pp. 744-752, June 2000.
- [35] S.B. Alexander, "Optical Communication Receiver Design," Bellingham, WA, SPIE Optical Engineering Press, 1997.
- [36] G.P. Agrawal, "Fiber-Optic Communication Systems, 3<sup>rd</sup> Edition," New York, NY, John Wiley & Sons, Inc, 1997.
- [37] Z. Ghassemlooy, "Pulse Interval Modulation for IR Communications," *Int. J. Commun. Syst.*, Special Issue, no.13, pp. 519-536, 2000.

- [38] L.M. Frass, W.E. Daniels, J. Muhs, "Infrared Photovoltaics for Combined Solar Lighting and Electricity for Buildings" Proc. 17<sup>th</sup> European Photovoltaic Solar Energy Conf, 1, 2001.
- [39] V.S. Hollis "Non-Invasive Monitoring of Brain Tissue Temperature by Near-Infrared Spectroscopy" M.S. Thesis, Chapter 3, University College London, 2002.
- [40] Krishnaswamy, G. Baranoski, "A study on skin optics," Technical Report. 2004 Jan;CS-2004-01.
- [41] G.M. Hale, M.R. Querry, "Optical constants of water in the 200 nm to 200  $\mu$ m wavelength region," Appl. Opt. vol. 12, pp. 555-563, 1973.
- [42] C.R. Simpson, M. Kohl, M. Essenpreis, M. Cope, "Near-infrared optical properties of ex vivo human skin and subcutaneous tissues measured using the Monte Carlo inversion technique," Phys. Med. Biol. vol. 43, pp. 2465-2478, 1998.
- [43] S.L. Jacques, D.J. McAuliffe, "The melanosome: threshold temperature for explosive vaporization and internal absorption coefficient during pulsed laser irradiation," Photochemistry and Photobiology, vol. 53, pp.769-75, 1991.
- [44] M.A. Everett, E. Yeagers, R.M. Sayre, R.L. Olson, "Penetration of Epidermis by Ultraviolet Rays," Photochemistry and Photobiology, vol. 5, pp. 533-542, 1966.
- [45] T.L. Troy, S.N. Thennadil, "Optical Properties of Human Skin in the Near-Infrared Wavelength Range of 1000 to 2200 nm," J of Biomedical Optics vol. 6, no. 2, pp. 167-176, 2001.
- [46] R.M.P Doornbos, R. Lang, M.C. Aalders, F.W. Cross, J.J.C.M. Sterenberg, "The determination of in vivo human tissue optical properties and absolute chromophore concentrations using spatially resolved steady-state diffuse reflectance spectroscopy," Phys. Med. Biol. vol. 44, pp. 967-981, 1999.
- [47] I.V. Meglinski, S.J. Matcher, "Quantitative assessment of skin layers absorption and skin reflectance spectra simulation in the visible and near-infrared spectral regions," Physiological Measurement, vol. 23, pp. 741-753, 2002.
- [48] Y. He, R.K. Wang, "Dynamic optical clearing effect of tissue impregnated with hyperosmotic agents and studied with optical coherence tomography," J Biomedical Optics, vol. 9, no. 1, pp. 200-206, Jan/Feb 2004.
- [49] G. Vargas, K.F. Chan, S.L. Thomsen, A.J. Welch, "Use of osmotically active chemical agents to alter the optical properties of tissue: Effects on the detected fluorescence signal measured through the skin," Lasers in Surgery and Medicine, vol. 29, pp. 213-220, 2001

- [50] Y. Ito, R.P. Kennan, E. Watanabe, H. Koizumi, "Assessment of heating effects in skin during continuous near infrared spectroscopy," *Journal of Biomedical Optics*, vol. 5, no. 4, pp. 383-390, 2000, Oct.
- [51] Bozkurt, B. Onaral, "Safety assessment of near infrared light emitting diodes for diffuse optical measurements," *Biomedical Engineering Online*, vol. 3, no.9, 2004.
- [52] B.P. Lathi, "Modern Digital and Analog Communication Systems, Third Edition," New York, NY, Oxford University Press, 1998.
- [53] Infrared Data Association, IrDA. "Infrared Data Association Serial Infrared Physical Layer Specification, Version 1.4". IrDA. 2001.
- [54] E. Zehavi, J.K. Wolf, "On Runlength Codes," *IEEE Trans. on Information Theory*, vol. 34, no. 1, pp. 45-54, 1998, Jan.
- [55] A.X. Widmer, P.A. Franaszek, "A DC-Balanced, Partitioned-Block, 8B/10B Transmission Code," *IBM Journal of Research and Development*, vol. 27, no. 5, pp. 440-451.
- [56] A.N. Coles, "A New 8B10B block code for high speed data transmission over unshielded twisted pair channels," *HP Labs Technical Reports*, HPL-96-142, 1996.
- [57] P. Sweeney, "Error control Coding: an Introduction," Hertfordshire, England, Prentice Hall International, 1991.